Neuromodulators generate multiple context-relevant behaviors in a recurrent neural network by shifting activity hypertubes

Ben Tsuda [1,2,3,*], Stefan C. Pate [1], Kay M. Tye [4], Hava T. Siegelmann [5], Terrence J. Sejnowski [1,6,7,*]

[1] Computational Neurobiology Laboratory, The Salk Institute for Biological Studies, La Jolla, CA 92037, USA
[2] Neurosciences Graduate Program, University of California San Diego, La Jolla, CA 92093, USA
[3] Medical Scientist Training Program, University of California San Diego, La Jolla, CA 92093, USA
[4] Systems Neuroscience Laboratory, The Salk Institute for Biological Studies, La Jolla, CA 92037, USA
[5] Biologically Inspired Neural & Dynamical Systems Laboratory, School of Computer Science, University of Massachusetts Amherst, Amherst, MA, 01003
[6] Institute for Neural Computation, University of California San Diego, La Jolla, CA 92093, USA
[7] Division of Biological Sciences, University of California San Diego, La Jolla, CA 92093, USA
[*] Correspondence: btsuda@salk.edu (B.T.), terry@salk.edu (T.J.S.)

Abstract

Mood, arousal, and other internal states can drastically alter behavior, even in identical external circumstances — a cold glass of water when you are thirsty is much more desirable than when you are sated. Neuromodulators are critical controllers of such neural states, with dysfunctions linked to various neuropsychiatric disorders. Although biological aspects of neuromodulation have been well studied, the computational principles underlying how large-scale neuromodulation of distributed neural populations shifts brain states remain unclear. We use recurrent neural networks to model how synaptic weight modulation — an important function of neuromodulators — can achieve nuanced alterations in neural computation, even in a highly simplified form. We find that under structural constraints like those in brains, this provides a fundamental mechanism that can increase the computational capability and flexibility of a neural network by enabling overlapping storage of synaptic memories able to generate diverse, even diametrically opposed, behaviors. Our findings help explain how neuromodulators "unlock" specific behaviors by creating task-specific hypertubes in the space of neural activities and motivate more flexible, compact and capable machine learning architectures.

Introduction

Neuromodulators are a central mechanism in the biological control of neural states that manifest as mood, arousal, and other variable behavioral modes [1, 2, 3, 4, 5, 6, 7]. Unlike standard, noise-sensitive models of context-dependent behaviors where exogenous cues are required to drive neurons [8] (Extended Data Fig. 1), neuromodulation can modify nearly every aspect of *how* neurons transduce information, including intrinsic ion channels and synaptic strengths using a scalar signal. This enables stable alterations of network computations over longer timescales that are robust to fluctuations in external inputs [9] (Extended Data Fig. 1), supporting neural states like sleep [3]. Pioneering studies on the lobster pyloric network [10, 11, 12] and other systems [13, 14] have revealed how neuron-specific neuromodulation can precisely tailor central pattern generator rhythms. Yet it remains unknown how large-scale neuromodulation of vast distributed neural populations can control global network dynamics and dictate behavior as it does in large brains.

Fully understanding neuromodulation in brains is important for several reasons. First, most psychiatric disorders either stem from or are directly related to neuromodulator dysregulation, as nearly all psychiatric drugs target neuromodulatory activity. Second, many of the psychiatric drugs currently in use only partially or imprecisely target neuromodulatory processes. Third, effects of many psychiatric treatments are highly variable, with some patients responding strongly and others failing to respond to multiple drugs. Fourth, neuromodulation acts via multiple mechanisms (as discussed below), allowing powerful circuit control but also making it difficult to fully understand how. Fifth, given the central role of neuromodulators in control of brains, a better understanding promises to make deep learning models based on brain architectures more flexible, more compact, and more efficient.

Neuromodulators affect several processes in brains including synaptic strengths, neural excitability, plasticity, and, indirectly, downstream circuit activity [15, 16, 10, 17]. Prior research has focused on different aspects of neuromodulation, including Yu and Dayan [18] who modeled the role of acetylcholine and norepinephrine in Bayesian probability estimations of uncertainties; Stroud et al. and Vecoven et al. [19, 20] who considered modulation of the neural activation function; Beaulieu et al.

[21] who formulated neuromodulation as a separate network that masks effector networks; Miconi et al. [22] who used modulation of synaptic plasticity to train networks; and Hasselmo et al. [23] who developed a model incorporating experimental work on multi-factor neuromodulator-specific circuit dynamics, particularly in hippocampal memory processes. Our model of synaptic weight modulation shares some similarities to previous models, particularly to the neural excitability models [19, 20]. Both lead to increased flexibility and versatility, yet they operate through independent mechanisms both biologically [16] and computationally (see Extended Data Appendix A).

We focus here on a critical aspect of neuromodulation in brains — synaptic weight modulation [10, 16, 13, 12, 24] — of which no general, biologically-plausible model exists. We consider a simplified approximation in which neuromodulators act as nearly uniform synaptic weight amplifiers or dampeners within a local region of a neural network. We show how this form of neuromodulation establishes overlapping synaptic memories corresponding to unique dynamic activity landscapes within a structurally-conserved neural network to generate unique behaviors. We demonstrate how neuromodulated circuits give rise to idiosyncratic, non-linear dose-response properties that can differ depending on the mode of neuromodulation. Using a well-established neuromodulation-mediated behavioral paradigm in *Drosophila*, we show how this form of neuromodulation naturally handles intermediate neural states, and as such, generalizes models of discrete internal state switching [25, 26] to continuous state transitions. Although many mechanisms may influence behavioral shifts, we show that a simple multiplicative factor applied to weights already acts as a powerful network control device, allowing neuromodulators to vastly increase the capability and complexity of computation in brains and making artificial neural networks more flexible, compact and capable.

Results

Neuromodulation creates multiple weight regimes within shared synaptic connections. The effects of neuromodulators on synaptic weights present a mode of circuit control [16] that is poorly understood in brains — both how it is implemented at scale and the computational mechanisms by which it shifts coordinated activity to generate different behaviors. Several recent studies

on cell type diversity have made clear that brains contain a complex array of neuromodulators that act with carefully coordinated spatiotemporal precision [27, 28, 29, 30, 31]. As a first step, we sought to assess whether a simplified form of neuromodulation — modelled as a uniform multiplicative factor acting on synaptic weights in a recurrent neural network (RNN) — could help us understand how neuromodulators control neural state. Although other modes of neural network control such as exogenous contextual cuing have been shown to successfully shift network behavior [8], uniform weight modulation represents a completely different biological and computational mechanism, which, given the complex, non-linear, and often unpredictable nature of RNNs, requires explicit assessment.

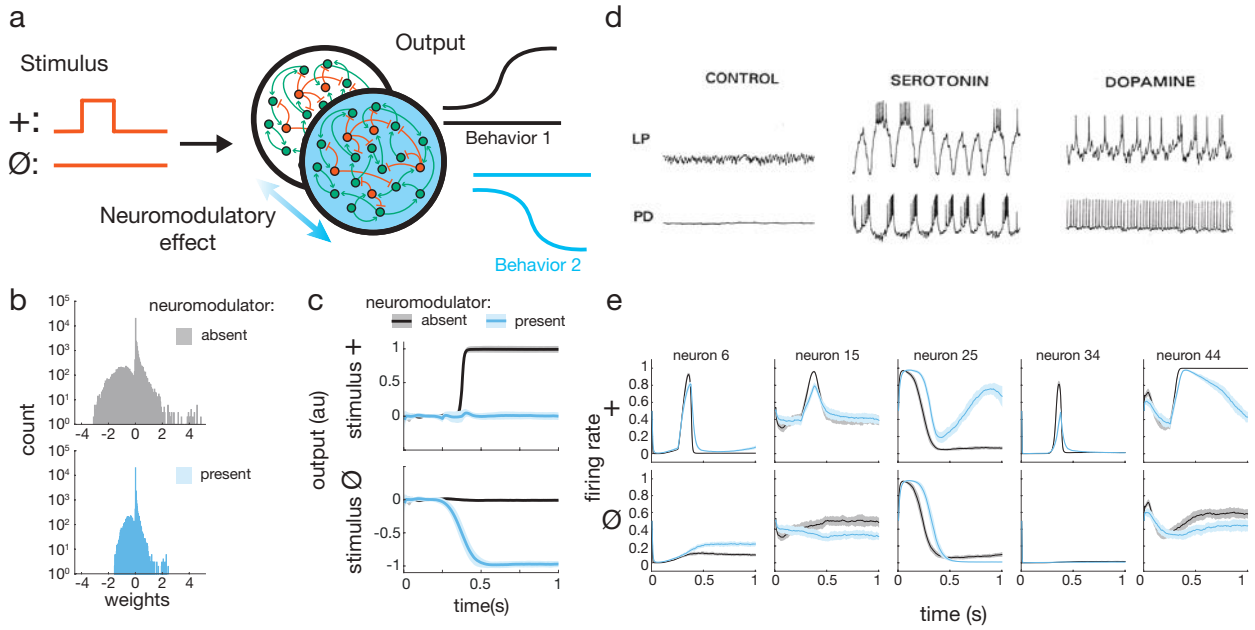

Fig. 1 | Neuromodulation weight scaling separates overlapping synaptic memory regimes. a, Modified Go-NoGo task. Given a stimulus (either + or ∅), in absence of neuromodulatory effect the recurrent neural network (RNN) should produce outputs from the Behavior 1 repertoire and in presence of neuromodulator, from Behavior 2. **b**, Approximation of neuromodulatory effect implemented in the model: all synaptic weights in the RNN are multiplied by a constant factor, here 0.5. **c**, Mean output to + and ∅ stimuli of 10 independently trained RNNs on the modified Go-NoGo with global neuromodulation factor 0.5. Shading represents standard deviation. **d**, Individual neuromodulators elicit unpredictable transforms of firing patterns in crustacean stomatogastric ganglion (STG) neurons. Reprinted from Neuron 76, Marder, Neuromodulation of Neuronal Circuits: Back to the Future, 1-11, 2012, with permission from Elsevier. **e**, Five example neurons' activity patterns from neuromodulated model RNN show complex nonlinear transformations analogous to crustacean STG activity changes under neuromodulation.

We used a modification of the classic Go, No Go experimental paradigm ("modified Go-NoGo;"

Fig. 1a; see Methods) to assess whether given identical input stimuli, uniformly shifting all the weights in a RNN — for example, scaling all weights by a factor of $\frac{1}{2}$ (Fig. 1b) — could elicit an independent behavior from the same network. We found that neuromodulation in this form was able to generate distinct behaviors for the task (Fig. 1c), demonstrating that this simple mechanism operating in brains can effectively separate synaptic memory regimes within a fixed circuit and access them through uniform scaling of weights to "unlock" specific behaviors (Extended Data Fig. 3). We found this result held over a wide range of neuromodulatory factors (Extended Data Fig. 4). Furthermore, reminiscent of neuromodulator effects on individual neuron activity patterns observed in lobster stomatogastric ganglion (Fig. 1d) and other organisms [10, 12, 32, 13], we found that both global activity (Extended Data Fig. 2a) and individual neuron activities were unpredictable, displaying non-linear transforms (Fig. 1e and Extended Data Fig. 2b).

Targeted neuromodulation can toggle across multiple global network states. In brains, neuromodulators are released in specific regions — some tightly localized, others broadcast widely — to influence local and global neural output. We found that RNNs with neuromodulated subpopulations of sizes across a broad range (100%–10% of the whole population) consistently supported the opposing behaviors of the task (Fig. 2a–c). Just as some neuromodulators affect neurons in a cell-type specific manner, for example selectively influencing activity of excitatory or inhibitory neurons with corresponding receptors [33], we found targeting of neuromodulator in this manner also was able to support the task (Fig. 2d,e).

To assess the flexibility of this neuromodulatory mechanism, we asked whether multiple unique behaviors could be learned and unlocked from a single network through targeted neuromodulation. Using an extended version of the modified Go-NoGo task (see Methods), we found that neuromodulation of distinct subpopulations or with distinct neuromodulation levels could support multiple behaviors, up to the maximum 9-behavioral Go-NoGo task we tested (Fig. 2f,g and Extended Data Figs. 5, 6; see Methods).

Distinct global network activity hypertubes with non-linear transition dynamics emerge from neuromodulation. To understand how this form of neuromodulation leads to network be-

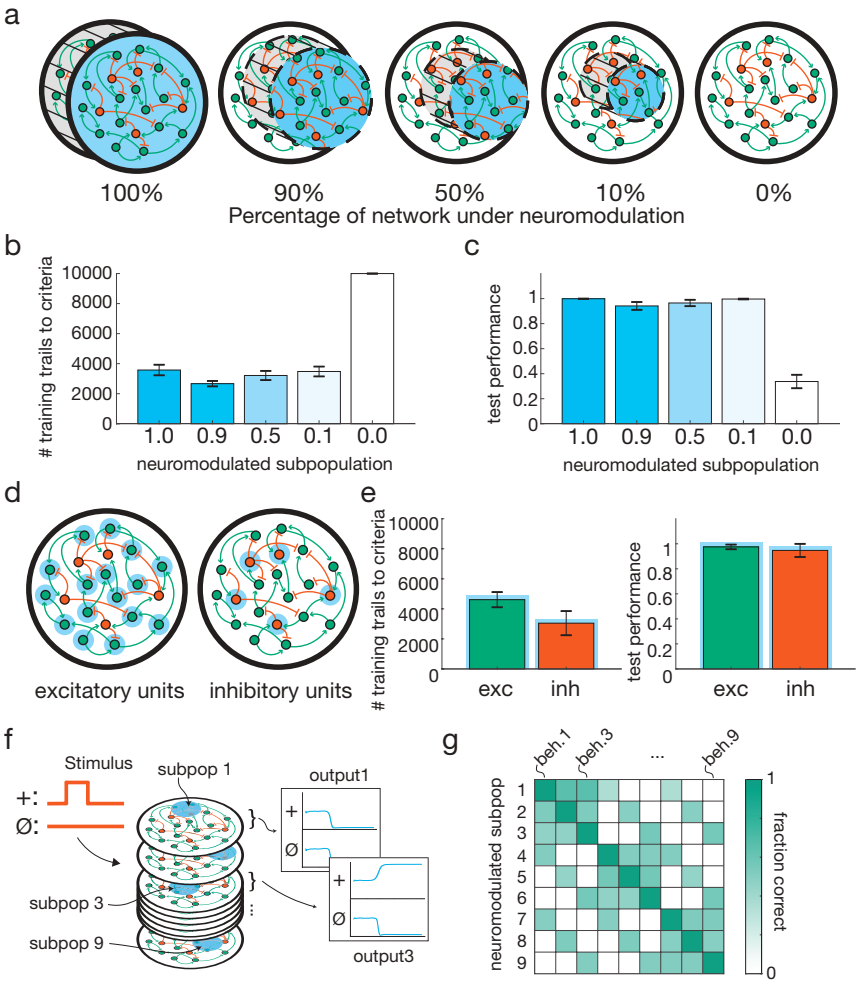

Fig. 2 | Targeted neuromodulation flexibly supports multiple behaviors. **a**, A range of different sized neural subpopulations embedded within a RNN were neuromodulated (factor (f_{nm}) = 0.5). 100% was positive control demonstrated in Fig. 1; 0% was negative control. **b**,**c**, RNNs with embedded neuromodulated subpopulations across the size spectrum could support the opposing behaviors of the modified Go-NoGo. **b**, Number of training trials to reach stop criteria (see Methods). **c**, Test performance (1 is 100% correct; see Methods). **d**, Neuromodulation of exclusively excitatory or inhibitory neurons (blue annuli). **e**, Excitatory or inhibitory neuromodulation supported learning of modified Go-NoGo. **f**, 9-behavior modified Go-NoGo task with unique neuromodulated subpopulations (subpops) and example corresponding outputs. **g**, RNNs successfully learned the task from **f** with 9 targeted subpops (each 10% of the RNN, non-overlapping; f_{nm}=2.5). Application of neuromodulator to any subpop unlocked a specific behavior set (beh.) from the 9-behavior repertoire (fraction of trials correct is ≈1 on diagonal; see Methods). Off-diagonal fraction correct due to partial output overlap between behavioral sets.

havior shifts, we analyzed the coordinated activity of all neurons in the RNN in the absence and presence of neuromodulator. At the individual neuron level, neuromodulation shifted the net difference of excitatory and inhibitory inputs, which in turn altered the recurrent propagation of activity over time and resultant internal network dynamics (Extended Data Figs. 7–9). At the whole population level, neural activity trajectories for the same stimulus with and without neuromodulator

followed non-overlapping, stereotyped paths, or hypertubes [34, 35, 36], in activity space (Fig. 3a). Through amplification of synaptic weights, neuromodulation effectively resets all the pins in the pinball machine, altering activity flow patterns through the RNN (Extended Data Fig. 1f and 10a).

The distinct hypertubes in activity space derive from a common underlying neural network. This suggests that there must be a transition between the hypertubes accessible through intermediate amounts of neuromodulation. To characterize this transition, we applied intermediate levels of neuromodulation to the RNN after training, which mapped a smooth transition from trajectories of the non-neuromodulated hypertube to those of the fully neuromodulated hypertube (Fig. 3b). Furthermore, intermediate neuromodulation generated intermediate outputs from the network (Fig. 3c). In this way, just as RNN neural trajectories have been shown to naturally address temporally varying sensory-motor patterns [34], neuromodulated neural trajectories provide a means to naturally respond to intermediate, even unexperienced neural states (e.g. hunger levels). To characterize the transition in output behavior, we measured the output of the RNN at the midpoint of each trial for each level of neuromodulation. We found that increasing neuromodulator levels led to non-linear (exponential or sigmoidal) progression from non-neuromodulated (Go: +1) to fully neuromodulated behavior (NoGo: 0) (Fig. 3d).

We next asked whether neuromodulatory transition dynamics were tightly constrained, defining a conserved property of neuromodulation, or highly variable depending on individual network characteristics. To test this, we independently trained 29 RNNs. All RNNs exhibited non-linear transition dynamics best fit by an exponential or sigmoid function (Fig. 3e and Extended Data Fig. 10b), but networks' sensitivities to neuromodulator and rates of transition varied drastically. To quantify this variability, we defined a "half maximal effective concentration" (EC50) as the amount of neuromodulator required to generate a half maximal output (see Methods). The EC50 of individual networks trained with a full neuromodulator factor of 9 ranged from 2.1 to 6.5 (3.1x range; Fig. 3f, left) and rate of transitions (steepness of the transition dynamics sigmoid) varied widely as well from 0.9 to 26.3 (Fig. 3f, right). This result reveals a previously unknown phenomenon that may contribute to the wide individual variability of neuropsychiatric drug sensitivities observed clinically [37]; a "circuit-based sensitivity."

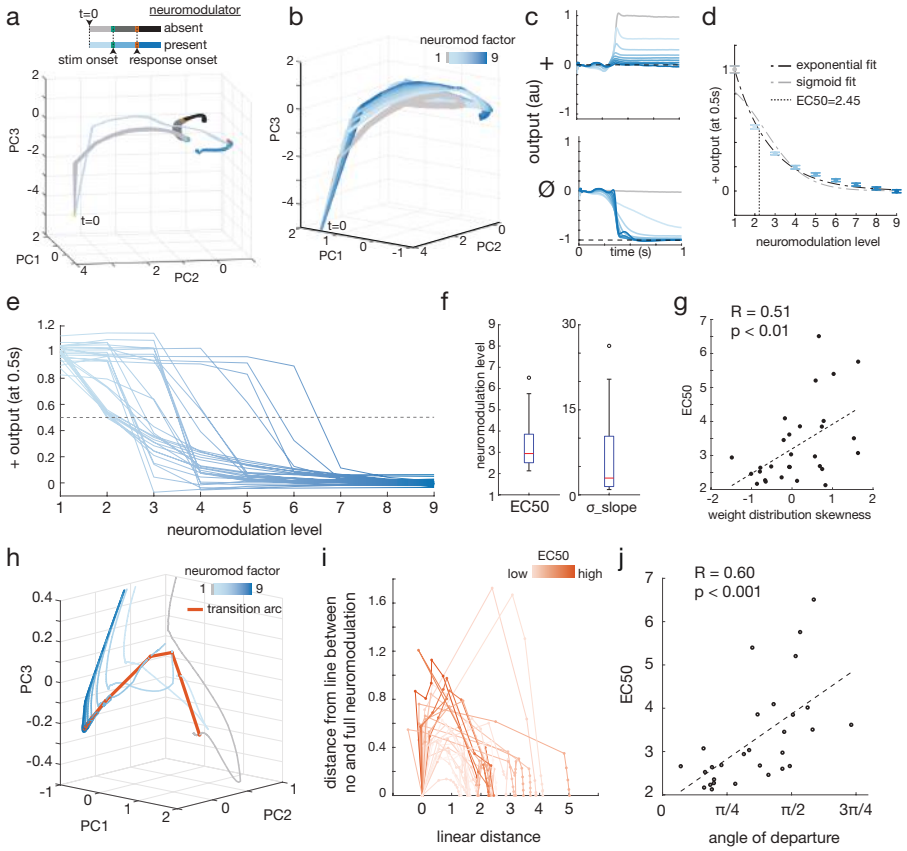

Fig. 3 | Neuromodulation separates activity hypertubes with idiosyncratic nonlinear transition dynamics. **a**, Global network activity dynamics after PCA-based dimensionality reduction for positive stimulus. Activity trajectories follow stereotyped, non-overlapping paths, or hypertubes in activity space. **b**, For a RNN trained with neuromodulatory factor of 9, intermediate levels of neuromodulation lead to partial transitions (traces in shades of blue) toward full neuromodulation activity hypertube (traces in darkest blue). **c**, Partial neuromodulation maps to intermediate output behaviors. **d**, Transition from none to full neuromodulation behavior is non-linear (best-fit exponential & sigmoid shown) and defines network sensitivity, measured as EC50. **e**, Output transition for 29 networks independently trained on the modified Go-NoGo task and tested across intermediate levels of neuromodulation. **f**, 29 independently trained RNNs exhibit large variability in transition dynamics, with EC50 ranging from 2.1 to 6.5 and sigmoid slope (σ_slope) from 0.9 to 26.3. **g**, Network EC50 is positively and significantly correlated with skewness of global weight distribution. **h**, Zoomed image demarcating path at a given timepoint over a network's neuromodulation transition manifold (orange; transition arc) which connects hypertubes corresponding to different neuromodulation levels in activity space (grey–blue trajectories). Blue shading same as in **b**. **i**, At a given timepoint (here t=100), intermediate levels of neuromodulation (represented by individual points) trace an arc between no neuromodulation (leftmost point on each curve) and full neuromodulation (rightmost point on each curve) states in phase space. Purely linear interpolation would lay along the x-axis at "distance from line (y-axis)" = 0. Each curve represents an individual network's transition arc across neuromodulation levels. Arcs are shaded by relative EC50. Arcs represent cross-section of full transition manifold connecting hypertubes across all timepoints at intermediate neuromodulation; each point on the arc is average of a cross section of a single hypertube. **j**, Angle of departure (angle formed between direct path and first neuromodulation level hypertube) exhibits a strong positive correlation with network EC50. Transition in direction more orthogonal or away from full neuromodulation state results in lower sensitivity, i.e. higher EC50.

We next sought to characterize what properties of the networks contribute to the variability in sensitivity to neuromodulator. We found that the skewness of networks' weight distributions exhibited a positive correlation with EC50s ($R=0.51$, $p<0.01$; Fig. 3g), suggesting networks with more positively skewed weights (longer tail of strong excitatory weights) were less sensitive to neuromodulator. To further understand the source of network sensitivity variability, we characterized the shape of the networks' activity transition curves across neuromodulation levels (Fig. 3h). At a given trial timepoint, purely linear interpolation yielded linear sensitivity relationships with invariant EC50 (Extended Data Fig. 11). In contrast, progressive neuromodulation defined an arc (Fig. 3h,i), which, collectively across all timepoints formed a curved transition manifold connecting each neuromodulation-specific activity hypertube. The geometry of this transition arc (measured as the angle of departure; see Methods) was strongly correlated to network sensitivity (Fig. 3j). This suggests that while individual networks can achieve identical performance on the trained task (no and full neuromodulation), the geometry of their population activities at intermediate neuromodulations is unique, leading to emergent sensitivity profiles.

Excessive neuromodulation can also occur either pathologically or pharmacologically. To model this, we applied neuromodulation at levels higher than those used during training and found neural dynamics could sometimes (but not always) diverge from trained activity hypertubes into an adjacent region of activity space, translating into inappropriate output behavior (Extended Data Fig. 10c–e).

Neuromodulated RNN replicates dopamine-mediated starvation-dependent sugar sensitivity in *Drosophila*. Given our finding that neuromodulation provides a natural means of handling intermediate, unexperienced neural states, we next sought to evaluate our model's ability to recapitulate the behavioral effects of neuromodulation observed *in vivo*. The neuromodulator dopamine controls the sugar sensitivity behavior of *Drosophila* [1], as measured by proboscis extension reflex (PER) probability, which increased with both duration of starvation (fed, 1 day, 2 day starved) and concentration of L-dopa administered in their diet (0, 3, 5 mg/ml) (Fig. 4a).

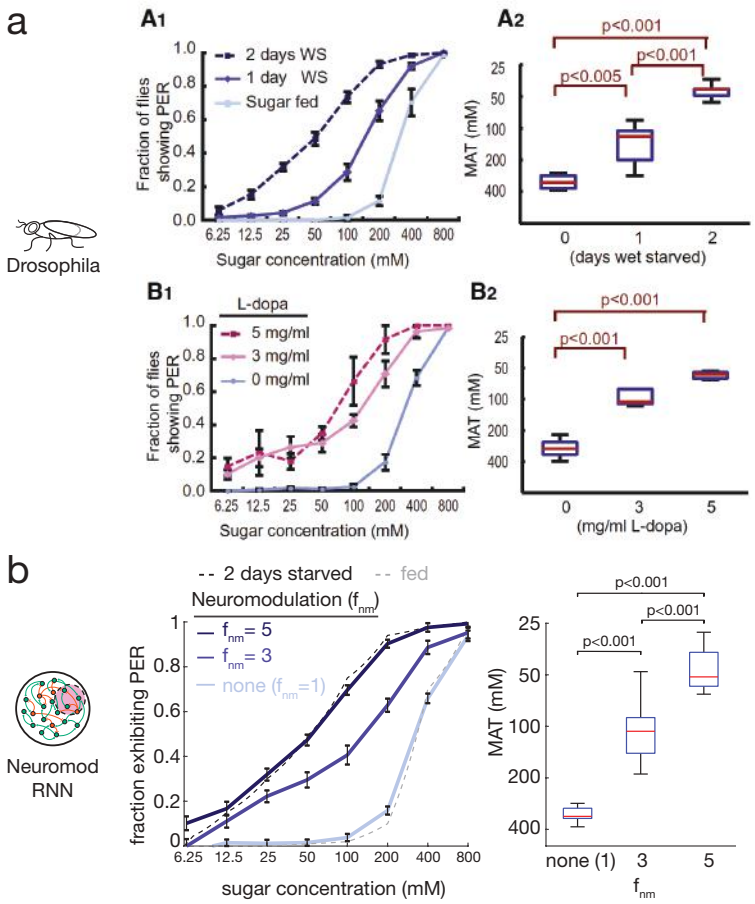

Fig. 4 | Neuromodulated RNNs reproduce *Drosophila* sugar sensitivity behaviors. a, *Drosophila* sugar sensitivity behaviors from Inagaki et al. 2012 measured as PER behavior vs sugar concentration. Reprinted from Cell 148, Inagaki et al., Visualizing Neuromodulation In Vivo: TANGO-Mapping of Dopamine Signaling Reveals Appetite Control of Sugar Sensing, 583-595, 2012, with permission from Elsevier. **b**, Neuromodulated RNNs trained on extremes of *Drosophila* sugar sensitivity (no neuromodulation factor (f_{nm}=1) for fed and f_{nm}=5 for 2 days starved) exhibit similar intermediate (f_{nm}=3; untrained) and extreme (no neuromodulation (f_{nm}=1) and f_{nm}=5; trained) behaviors (n=10; error bars are SEM; same statistical test as in Inagaki et al. 2012 for boxplots, see Methods).

To assess if our neuromodulation model could reproduce these results, we trained RNNs with neuromodulated subpopulations (20% subpopulation) to reproduce the fed and 2 day starved sugar sensitivity curves of flies (no neuromodulation (f_{nm}=1) for fed; f_{nm}=5 for 2 day starved). We then tested the RNNs' behaviors at an intermediate, never-before experienced neuromodulator level (f_{nm}=3). The RNNs produced a shifted sensitivity curve very similar to that exhibited by 1 day starved flies and the flies fed an intermediate L-dopa concentration of 3 mg/ml (Fig. 4b).

The behavior of the RNNs reliably mimicked the intermediate behaviors of flies *in vivo* because

intermediate neuromodulation caused a continuous shift in the RNN's activity hypertube between "fed" and "2 day starved/5 mg/ml L-dopa" hypertubes (Extended Data Fig. 12a–c). Furthermore, our model reveals that transition manifolds (defined by the hypertubes connecting intermediate neuromodulation levels) are unique to networks, predicting wide-ranging natural variability in fly starvation-based sugar sensitivity profiles (Extended Data Fig. 12d). Neuromodulation leads to natural handling of never-before experienced neural states by creating a network configuration such that the neuromodulatory transition manifold has a geometry that leads to intermediate outputs.

Electrical modulation shifts neural dynamics through an independent circuit effect. Other endogenous and exogenous influences can alter neural circuit dynamics through mechanisms that may be shared or independent, and understanding relationships between such interventions is vital for safe and effective treatment. We used our model to compare whether exogenously delivered electrical modulation of a neuromodulated circuit — analogous to use of optogenetics experimentally [38] and deep-brain stimulation (DBS) and transcranial magnetic stimulation clinically [39, 40, 41] — alters network activity in an analogous manner to chemical neuromodulation or operates through an independent effect (Fig. 5a).

We computationally applied electrical modulation (excitatory or inhibitory current; see Methods) to RNNs trained with neuromodulated subpopulations and found that while electrical current given to random subpopulations did not affect the RNNs' performances, current delivered to the neuromodulated subpopulation could significantly affect network output (Fig. 5b), shifting behaviors directionally toward the opposing neuromodulation condition behavioral set (Extended Data Fig. 13a,b).

In each RNN, increasing the level of targeted electrical input — for example inhibitory modulation in the absence of neuromodulator — led to a graded transition in behavior similar to the transition observed with graded administration of neuromodulator (Fig. 5c). To compare these conditions, we measured the amount of electrical input that led to output of 50% of the fully-neuromodulated condition (e-mod$_{50}$) analogous to EC50 for neuromodulator levels. Interestingly, RNNs also exhibited idiosyncratic circuit-based sensitivity to electrical modulation, with e-mod$_{50}$ under inhibitory

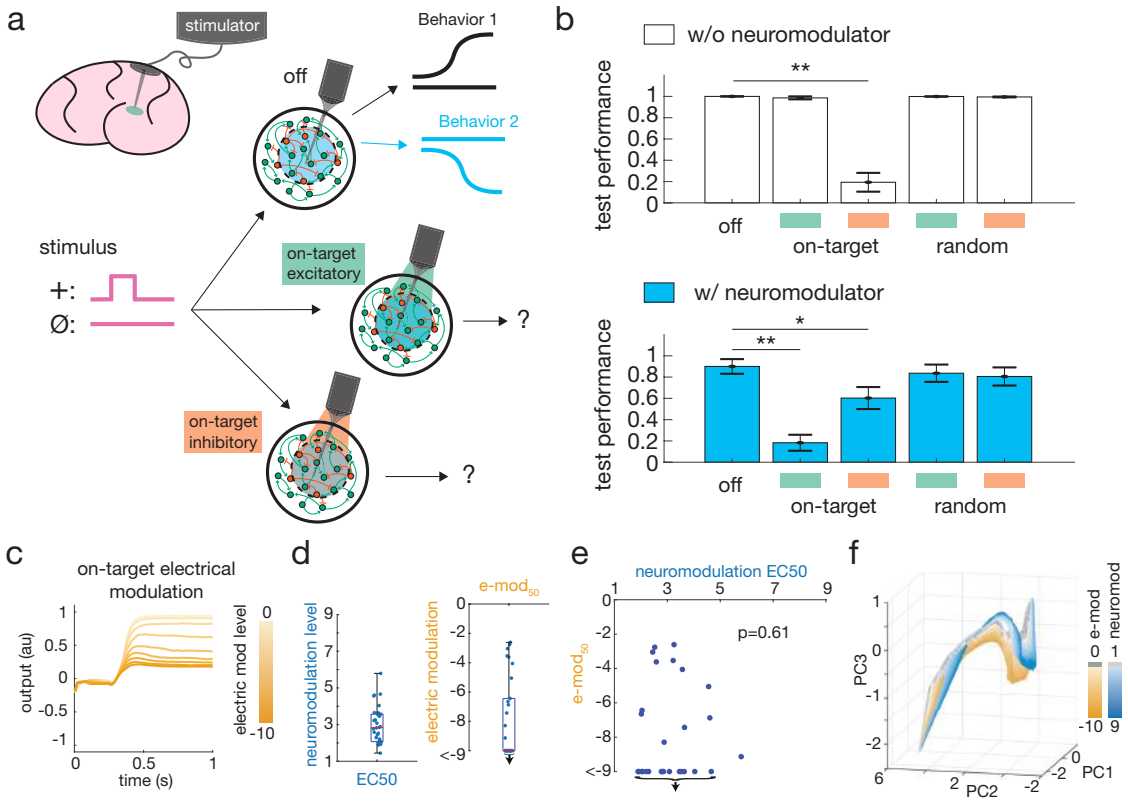

Fig. 5 | Targeted electrical modulation shifts network dynamics through independent circuit effect. **a**, Schematic of DBS and analogous electrical modulation (e-mod) of a neuromodulated RNN. **b**, Test performance was significantly impaired in absence of neuromodulation (white bars) when inhibitory on-target electrical modulation (e-mod) was given (p=3.91e-11) and with neuromodulation (blue bars) when excitatory and inhibitory on-target e-mod was given (p=2.20e-08 and p=2.18e-02, respectively). *:p<0.05, **:p<0.01. **c**, RNN output in absence of neuromodulation to + stimulus with increasing inhibitory e-mod. **d**, For 30 RNNs: Left: neuromodulation EC50. Right: electrical e-mod$_{50}$. Down arrows in **d**, **e** indicate RNNs that did not achieve e-mod$_{50}$ at maximum stimulation. **e**, No significant correlation between networks' EC50 and e-mod$_{50}$. **f**, Neuromodulation and electrical modulation push activity trajectories along different transition manifolds enabling independent transition dynamics.

modulation ranging from -2.6 input current to not achieving e-mod$_{50}$ by the maximum modulation we administered (-9 input current; >3.5x range) (Fig. 5d, right).

We then assessed whether networks' electrical and chemical sensitivities were related, and found no significant correlation (Fig. 5e). Since some RNNs' outputs did not reach e-mod$_{50}$, saturating before the maximum electrical input given, — further evidence of a different mechanism at play — we also measured each RNN's output at maximum electrical input (input=-9) and similarly found no significant correlation to EC50 (Extended Data Fig. 13c). The lack of correlation suggests that networks insensitive to chemical modulation may still be highly sensitive to electrical modulation

and vice versa. Consistent with this, we found that electrical modulation progressively shifted population dynamics along a manifold transition distinct to neuromodulation, enabling different rates of transition (Fig. 5f). This may help explain why some patients who fail pharmacologic treatments sometimes respond dramatically to DBS. By utilizing an independent mechanism to chemical modulation, DBS exploits a parallel circuit-sensitivity to achieve therapeutic efficacy.

Discussion

Neuromodulation in brains drives unique neural function in health and disease. Using an RNN model, we showed how neuromodulators, through simple scaling of synaptic weights, can generate unique behavioral modes from a single RNN. The importance of our findings is not that our model was able to solve tasks like Go, No Go, which other computational models with mechanisms like contextual cuing can also solve. Rather, we showed how neuromodulation, a completely independent and previously uncharacterized control mechanism that is highly relevant biologically and clinically, is able to rapidly reconfigure a network with only a single scalar input.

Our model provides insights into neuromodulation that are related to other recently elucidated principles of neural computation. We showed that neuromodulation leads to separation of distinct activity hypertubes, similar to those observed by Goudar and Buonomano [34] and Nieh et al. [36], with neuromodulation effectively disentangling neural trajectories by separating them in phase space analogous to the work of Russo et al. [42] in motor cortex. Just as neural trajectories provide transformations in phase space that naturally handle temporal variation of sensory-motor patterns [34], neuromodulation leads to transformations in phase space that elucidate a biological mechanism for handling intermediate and continuously transitioning neural states, even if never experienced before. We demonstrated the biological use of this property through replication of Inagaki et al.'s findings in *Drosophila* [1]. In this way, the level of neuromodulation acted as a controller on the amount of disentangling of neural trajectories, using internal neural state (amount of weight modulation) to control output behavior. Such a system is robust to external noise (Extended Data Fig. 1), since far apart neural states generate trajectories that are widely separated in phase space.

Through this analysis we discovered a feature of networks previously unreported to our knowledge: "circuit-based sensitivity," which helps explain the clinical observation of high variability in drug and other therapeutic response [37], alongside more standard explanations like enzyme variant-dependent drug metabolism and clearance rates. This emergent sensitivity property of neuromodulated networks is related to the well-known "many solutions" phenomenon of neural networks where different weight configurations can produce identical output [43, 44]. Unlike studies focusing on variability in networks producing identical output, our model allowed study for the first time of the transition dynamics under neuromodulation, revealing unique geometric configurations of phase space underlying emergent network sensitivity profiles.

Future studies aimed at identifying circuit parameters that control this transition dynamic geometry will be critical for understanding and use in therapeutic optimization. The idiosyncratic nature of circuit-based sensitivity aligns with current efforts in precision medicine calling for the need to consider each patient as an idiosyncratic individual — here we provide computational evidence for this claim and its particular importance in neuropsychiatric treatment [45]. Fully understanding the relationship between chemical and electrical modulation and sensitivity is also crucial. Although our simplified model suggests how the modes of modulation influence dynamics (see Extended Data Appendix B), further analytical and experimental investigation into their relationship as network dynamics evolve over time could provide deeper insights.

Our formulation of the neuromodulatory effect on synaptic weights is a simplification of the true biological mechanism. Elaborating our model to support differential weight modulation (e.g. via multiple neuromodulators and neuromodulator receptor subtypes on specific cell-types) [46, 4], neuromodulator multiplexing [33, 30], and metamodulation [16, 47, 6] will likely lead to even more sophisticated network behavior. Our model also uses arbitrary neuromodulation levels, whereas brains likely use specific levels for optimal functionality. Future investigation into which levels are optimal and methods of learning these will be important.

Finally, neuromodulation provides interesting directions for machine learning (ML). By separating

synaptic memory regimes in a single network, we demonstrate how a network can have much greater flexibility and increased capacity, supporting a library of unique behaviors for overlapping external contingencies. Furthermore, each behavior can be rapidly accessed through targeted application of the relevant neuromodulatory factor. High capacity, compact networks with high-speed access to different output modes presents a promising component for ML development and storage-limited applications like edge computing. Additionally, through the separation of memory regimes that effectively splits a single RNN into multiple processors, this mechanism may provide a means of realizing the super-Turing capability of specific RNN configurations as defined by Cabessa and Siegelmann [48]. Future theoretical assessment of neuromodulated RNNs' capacity will establish if this simple mechanism is sufficient to exceed the Turing limit.

Acknowledgements

We thank Y. Chen and R. Kim for helpful discussions and feedback on the manuscript. We thank J. Aldana for support with computing resources. This work was supported by the Kavli Institute for Brain and Mind at University of California San Diego, Office of Naval Research Grant N00014-16-1-2829, Defense Advanced Research Projects Agency Grant HR0011-18-2-002, National Institute of Mental Health Grant R37-MH102441, and National Center for Complementary and Integrative Health Pioneer Award DP1-AT009925.

Author contributions

B.T., K.M.T., H.T.S., and T.J.S. formulated the ideas. B.T. and S.C.P. performed the simulations and analyses. B.T., S.C.P, K.M.T., H.T.S., and T.J.S. wrote the manuscript.

Declaration of interests

The authors declare no competing interests.

References

[1] Inagaki, H. K. *et al.* Visualizing neuromodulation in vivo: Tango-mapping of dopamine signaling reveals appetite control of sugar sensing. *Cell* **148**, 583–595 (2012).

[2] Burgos-Robles, A. *et al.* Amygdala inputs to prefrontal cortex guide behavior amid conflicting cues of reward and punishment. *Nature Neuroscience* **20**, 824–835 (2017).

[3] A.McCormick, D., Nestvogel, D. B. & He, B. J. Neuromodulation of brain state and behavior. *Annual Review of Neuroscience* **43**, 391–415 (2020).

[4] Bacqué-Cazenave, J. *et al.* Serotonin in animal cognition and behavior. *International Journal of Molecular Sciences* **21**, 1649 (2020).

[5] Avery, M. C. & Krichmar, J. L. Neuromodulatory systems and their interactions: A review of models, theories, and experiments. *Frontiers in Neural Circuits* **11**, 108 (2017).

[6] Katz, P. S. & Edwards, D. H. Metamodulation: the control and modulation of neuromodulation. In Katz, P. S. (ed.) *Beyond Neurotransmission: Neuromodulation and its Importance for Information Processing*, chap. 10, 349–381 (Oxford University Press, Oxford, UK, 1999).

[7] Allen, W. E. *et al.* Thirst regulates motivated behavior through modulation of brainwide neural population dynamics. *Science* **364**, eaav3932 (2019).

[8] Mante, V., Sussillo, D., Shenoy, K. V. & Newsome, W. T. Context-dependent computation by recurrent dynamics in prefrontal cortex. *Nature* **503**, 78–84 (2013).

[9] Haddad, S. A. & Marder, E. Circuit robustness to temperature perturbation is altered by neuromodulators. *Neuron* (2018).

[10] Marder, E. Neuromodulation of neuronal circuits: Back to the future. *Neuron* **76**, 1–11 (2012).

[11] Marder, E. & Eisen, J. S. Electrically coupled pacemaker neurons respond differently to same physiological inputs and neurotransmitters. *Journal of Neurophysiology* **51**, 1362–1374 (1984).

[12] Johnson, B. R., Peck, J. H. & Harris-Warrick, R. M. Distributed amine modulation of graded chemical transmission in the pyloric network of the lobster stomatogastric ganglion. *Journal of Neurophysiology* **74**, 437–452 (1995).

[13] Katz, P. S., Getting, P. A. & Frost, W. N. Dynamic neuromodulation of synaptic strength intrinsic to a central pattern generator circuit. *Nature* **367**, 729–731 (1994).

[14] Jing, J., Gillette, R. & Weiss, K. R. Evolving concepts of arousal: Insights from simple model systems. *Reviews in the Neurosciences* **20**, 405–427 (2009).

[15] Newman, E. L., Gupta, K., Climer, J. R., Monaghan, C. K. & Hasselmo, M. E. Cholinergic modulation of cognitive processing: insights drawn from computational models. *Frontiers in Behavioral Neuroscience* **6**, 24 (2012).

[16] Nadim, F. & Bucher, D. Neuromodulation of neurons and synapses. *Current Opinion in Neurobiology* **29**, 48–56 (2012).

[17] Weele, C. M. V. *et al.* Dopamine enhances signal-to-noise ratio in cortical-brainstem encoding of aversive stimuli. *Nature* **563**, 397–401 (2018).

[18] Yu, A. J. & Dayan, P. Uncertainty, neuromodulation, and attention. *Neuron* **46**, 681–692 (2005).

[19] Stroud, J. P., Porter, M. A., Hennequin, G. & Vogels, T. P. Motor primitives in space and time via targeted gain modulation in cortical networks. *Nature Neuroscience* **21**, 1774–1783 (2018).

[20] Vecoven, N., Ernst, D., Wehenkel, A. & Drion, G. Introducing neuromodulation in deep neural networks to learn adaptive behaviors. *Plos One* **15**, e0227922 (2020).

[21] Beaulieu, S. *et al.* Learning to continually learn. In Giacomo, G. D. *et al.* (eds.) *24th European Conference on Artificial Intelligence (ECAI)*, vol. 325, 992–1001 (IOS Press, Santiago de Compostela, Spain, 2020).

[22] Miconi, T., Rawal, A., Clune, J. & Stanley, K. O. Backpropamine: training self-modifying neural networks with differentiable neuromodulated plasticity. In *7th International Conference on Learning Representations, ICLR 2019, New Orleans, LA, USA, May 6-9, 2019* (2019).

[23] Hasselmo, M. E., Schnell, E. & Barkai, E. Dynamics of learning and recall at excitatory recurrent synapses and cholinergic modulation in rat hippocampal region ca3. *Journal of Neuroscience* **15**, 5249–5262 (1995).

[24] Hasselmo, M. E. The role of acetylcholine in learning and memory. *Curr Opin Neurobiol.* **16**, 710–715 (2006).

[25] Calhoun, A. J., Pillow, J. W. & Murthy, M. Unsupervised identification of the internal states that shape natural behavior. *Nature Neuroscience* **22**, 2040–2049 (2019).

[26] Cermak, N. *et al.* Whole-organism behavioral profiling reveals a role for dopamine in state-dependent motor program coupling in c. elegans. *eLife* **9**, e57093 (2020).

[27] Xie, P. *et al.* Morphological diversity of single neurons in molecularly defined cell types. *Nature* **598**, 174–181 (2021).

[28] Radnikow, G. & Feldmeyer, D. Layer- and cell type-specific modulation of excitatory neuronal activity in the neocortex. *Frontiers in Neuroanatomy* **12** (2018).

[29] Zhang, S. X. *et al.* Hypothalamic dopamine neurons motivate mating through persistent camp signalling. *Nature* **597**, 245–249 (2021).

[30] Li, X., Bucher, D. & Nadim, F. Distinct co-modulation rules of synapses and voltage-gated currents coordinate interactions of multiple neuromodulators. *Journal of Neuroscience* **38**, 8549–8562 (2018).

[31] Patriarchi, T. *et al.* Ultrafast neuronal imaging of dopamine dynamics with designed genetically encoded sensors. *Science* **360**, eaat4422 (2018).

[32] Johnson, B. R. *et al.* Differential modulation of synaptic strength and timing regulate synaptic efficacy in a motor network. *Journal of Neurophysiology* **105**, 293–304 (2011).

[33] Wester, J. C. & McBain, C. J. Behavioral state-dependent modulation of distinct interneuron subtypes and consequences for circuit function. *Current Opinion in Neurobiology* **29**, 118–125 (2014).

[34] Goudar, V. & Buonomano, D. V. Encoding sensory and motor patterns as time-invariant trajectories in recurrent neural networks. *eLife* **7**, e31134 (2018).

[35] Low, R. J., Lewallen, S., Aronov, D., Nevers, R. & Tank, D. W. Probing variability in a cognitive map using manifold inference from neural dynamics. *bioRxiv* (2018). URL `https://doi.org/10.1101/418939`.

[36] Nieh, E. H. *et al.* Geometry of abstract learned knowledge in the hippocampus. *Nature* (2021).

[37] Furukawa, T. A. *et al.* Optimal dose of selective serotonin reuptake inhibitors, venlafaxine, and mirtazapine in major depression: a systematic review and dose-response meta-analysis. *Lancet Psychiatry* **6**, 601–609 (2019).

[38] Deisseroth, K. Optogenetics: 10 years of microbial opsins in neuroscience. *Nature Neuroscience* **18**, 1213–1225 (2015).

[39] Krauss, J. K. *et al.* Technology of deep brain stimulation: current status and future directions. *Nature Reviews Neurology* **17**, 75–87 (2021).

[40] Risio, L. D. *et al.* Recovering from depression with repetitive transcranial magnetic stimulation (rTMS): a systematic review and meta-analysis of preclinical studies. *Translational Psychiatry* **10**, 393 (2020).

[41] Gouveia, F. V. *et al.* Neuromodulation strategies in post-traumatic stress disorder: From preclinical models to clinical applications. *Brain Sciences* **9**, 45 (2019).

[42] Russo, A. A. *et al.* Motor cortex embeds muscle-like commands in an untangled population response. *Neuron* **97**, 953–966 (2018).

[43] Mehrer, J., Spoerer, C. J., Kriegeskorte, N. & Kietzmann, T. C. Individual differences among deep neural network models. *Nature Communications* **11**, 5725 (2020).

[44] Maheswaranathan, N., Williams, A. H., Golub, M. D., Ganguli, S. & Sussillo, D. Universality and individuality in neural dynamics across large populations of recurrent networks. In *Advances in Neural Information Processing Systems 32, NeurIPS* (2019).

[45] Provenza, N. R. *et al.* The case for adaptive neuromodulation to treat severe intractable mental disorders. *Frontiers in Neuroscience* **13**, 152 (2019).

[46] Harris-Warrick, R. M. & Johnson, B. R. Checks and balances in neuromodulation. *Frontiers in Behavioral Neuroscience* **4**, 47 (2010).

[47] Ribeiro, J. A. & Sebastiao, A. M. Modulation and metamodulation of synapses by adenosine. *Acta Physiologica* **199**, 161–169 (2010).

[48] Cabessa, J. & Siegelmann, H. T. The super-Turing computational power of plastic recurrent neural networks. *International Journal of Neural Systems* **24**, 1450029 (2014).

[49] Kim, R. & Sejnowski, T. J. Strong inhibitory signaling underlies stable temporal dynamics and working memory in spiking neural networks. *Nature Neuroscience* **24** (2020).

[50] Trujillo, C. A. *et al.* Pharmacological reversal of synaptic and network pathology in human MECP2-KO neurons and cortical organoids. *EMBO Molecular Medicine* **13**, e12523 (2020).

[51] Song, H. F., Yang, G. R. & Wang, X.-J. Training excitatory-inhibitory recurrent neural networks for cognitive tasks: A simple and flexible framework. *PLOS Computational Biology* **12**, 1–30 (2016).

[52] Kim, R., Li, Y. & Sejnowski, T. J. Simple framework for constructing functional spiking recurrent neural networks. *PNAS* **116**, 22811–22820 (2019).

[53] Laje, R. & Buonomano, D. V. Robust timing and motor patterns by taming chaos in recurrent neural networks. *Nature Neuroscience* **16**, 925–933 (2013).

[54] Cunningham, J. P. & Yu, B. M. Dimensionality reduction for large-scale neural recordings. *Nature Neuroscience* **17**, 1500–1508 (2014).

Methods

Modified Go-NoGo tasks. The classic Go-NoGo task has two possible stimuli (positive pulse referred to as positive stimulus or +; no pulse, also referred to as null stimulus or $\emptyset$). The agent is trained to give a positive output (+1, "Go") for the positive stimulus and zero output (0, "NoGo") for the null stimulus. In the modified Go-NoGo task we added a second possible behavioral set: NoGo for the positive stimulus and negative output (-1, "AntiGo") for the null stimulus. The network was trained on the classic Go-NoGo behavior in the absence of neuromodulator and on the new NoGo-AntiGo behavior in the presence of neuromodulator. The 3 behavior and 9 behavior variants of the modified Go-NoGo task followed a similar paradigm with additional added behaviors. In the 3 behavior version, a third behavior of positive stimulus $\rightarrow$ AntiGo, null stimulus $\rightarrow$ Go was added. In the 9 behavior version all possible stimulus $\rightarrow$ output response pairs were added. As such, Behavior 1 was $+ \rightarrow$ AntiGo, $\emptyset \rightarrow$ AntiGo; Behavior 2 was $+ \rightarrow$ NoGo, $\emptyset \rightarrow$ AntiGo; Behavior 3 was $+ \rightarrow$ Go, $\emptyset \rightarrow$ AntiGo; ...; Behavior 9 was $+ \rightarrow$ Go, $\emptyset$ Go. In our simulations each trial lasted 200 timesteps of 5ms each for a total represented duration of 1 second.

Neuromodulatory neural network model. For our simulations we used a continuous rate recurrent neural network (RNN) model with biologically plausible parameters similar to RNNs in prior works [49, 50]. Consistent with biological neural networks, we implemented Dale's Law using

the method in Song et al. [51] such that each neuron was either excitatory or inhibitory. For all our simulations we used a RNN with $N = 200$ neuron units, 80% excitatory and 20% inhibitory. In the RNN each neuron can be connected to any other neuron with probability p_{con} (p_{con} was initialized at 0.8 in our simulations), and each neuron receives weighted input from connected neurons to produce a firing rate governed by the neural dynamical equation

$$\boldsymbol{\tau}\frac{d\boldsymbol{x}}{dt} = -\boldsymbol{x} + W\boldsymbol{r} + W_{in}u + N(0, 0.1) \tag{1}$$

where $\boldsymbol{\tau} \in R^{1\times N}$ is the synaptic decay time constant for the N neurons in the network, $\boldsymbol{x} \in R^{1\times N}$ is the synaptic current variable for the N neurons, $W \in R^{N\times N}$ is the matrix of synaptic weights between all N neurons, $\boldsymbol{r} \in R^{1\times N}$ is the output firing rates of the N neurons in the network, $W_{in} \in R^{1\times N}$ are weights associated with external input u, and $N(0, 0.1)$ is added noise drawn from a normal distribution with mean 0 and variance 0.1. The output firing rate for the neurons is given by an elementwise nonlinear transfer function transformation of the synaptic current variable. In our network we used the standard logistic sigmoid function as implemented by prior models [52, 49]:

$$\boldsymbol{r} = \frac{1}{1 + e^{-\boldsymbol{x}}} \tag{2}$$

The synaptic connectivity matrix W was randomly initialized from a normal distribution with zero mean and standard deviation $g/\sqrt{N \cdot p_{con}}$, where g is the gain. We set $g = 1.5$ as previous studies have shown that networks operating in a high gain regime ($g \geq 1.5$) support rich dynamics analogous to those of biological networks [49, 52, 53]. The synaptic decay time constants were randomly initialized to a value in the biologically plausible range of 20–100 ms. As in Kim et al. 2019, we used the first-order Euler approximation method to discretize equation (1) for the simulations; for neuron i:

$$x_{i,t} = (1 - \frac{\Delta t}{\tau})x_{i,t-1} + \frac{\Delta t}{\tau}(\sum_j W_{ji}r_{ji,t-1} + W_{ui}u_{t-1}) + N(0, 0.1) \tag{3}$$

Output was generated by taking all recurrent network neurons' activities and passing them through

a weighted output unit

$$o_{network} = W_{out}\boldsymbol{r} + b_{out}$$

where $W_{out} \in R^{N\times 1}$ are the neural output weights and b_{out} is the output unit's bias term. RNNs were trained by backpropagation through time using AdamOptimizer with a least square error objective function.

To apply an amplifying or dampening neuromodulatory effect, target neurons' weights were scaled by the neuromodulatory factor. For whole network neuromodulation this effect was applied to all neurons in the RNN; for subpopulation neuromodulation the effect was applied only to the selected subpopulation of neurons.

For the modified Go-NoGo task, RNNs were trained until one of two possible stop criteria was met: 1) average trial least square error over the last 50 trials was under a threshold of 1, or 2) 10,000 training trials was reached. Performance on the task was then assessed by evaluating the percentage of test trials that matched the following performance criteria: for Go trials, output was required to reach 1.0 ± 0.2 by timestep 120 (full trial was 200 timesteps); for NoGo trails, output was required to be 0.0 ± 0.2 and for AntiGo trails -1.0 ± 0.2 at timestep 120.

Comparison to context-dependent cued model. For comparison, we created a cue-driven RNN model and trained it on the Modified Go-NoGo task. The cue, which we refer to as the "context cue", was delivered through an additional input channel and signaled which output behavior was desired. We created models with two types of cues: transient cues were constant value inputs present only during the stimulus input period (t=0 to t=75); persistent cues were constant value inputs across the whole trial. For comparisons between models, we ran models with cue pairs of +1.0/-1.0 (2.0 sep in Extended Data Fig. 1d,e), +0.5/-0.5 (1.0 sep), and +0.2/-0.2 (0.4 sep).

To compare the neuromodulatory and context-cued RNNs tolerance to noise, we ran two types of simulation experiments. First, we added Gaussian noise of zero mean and standard deviation

ranging from 0 to 4 to all input signals and measured RNN performance as the difference between target and actual output. At each level of noise, we simulated 4 independent models 100 times each and averaged their performances (Extended Data Fig. 1d). In a second experiment, after training, we simulated pure intrinsic network activity (no inputs). We again added Gaussian noise of zero mean and standard deviation ranging from 0 to 4. For each batch of 100 simulations on 4 replicate networks, we examined the consistency of final network states (t=200). To measure this, we computed the mean Euclidean distance of the 100 simulations final-time-step states from the centroid, giving a measure of final network state spread. Larger mean Euclidean distance (higher spread) indicated more variable activity trajectories; lower mean distance (lower spread) indicated highly consistent activity trajectories (Extended Data Fig. 1e).

The phase portraits with flow fields were created by simulating a network to produce two state trajectories from distinct behavioral contexts. For this we used a neuromodulatory network (f_{nm}=9) and a context-cued model with persistent cues 0/+2.0. For each network configuration (with and without neuromodulator, and cued model), we computed the derivative of the neurons' rates across the trajectories to generate vector fields depicting the intrinsic flow fields of the network in the absence of any driving input. For the exogenously cued model, we then calculated the external drive required across the alternative cue-driven trajectory (cue=+2.0) to achieve the corresponding activity trajectory. We projected state trajectories and flow fields into the first three PCA space for visualization (Extended Data Fig. 1f).

Neuromodulation of multiple subpopulations and multiple levels. For neuromodulation of non-overlapping subpopulations, same-sized groups of neurons were choosen randomly without any overlap and neuromodulator applied to each for a given behavior. For overlapping subpopulations, groups of neurons were chosen randomly allowing overlap (Extended Data Fig. 6).

Neuromodulation at different levels ("multi-factor networks") was done by applying different neuromodulation factors (f_{nm}). For the 9-behavior modified Go-NoGo this was done using factors $\in [1:1:9]$, i.e., for Behavior 1 no factor was applied ($f_{nm} = 1$), for Behavior 2 $f_{nm} = 2$, for Behavior 3 $f_{nm} = 3$, et cetera.

To test networks across the range of subpopulation sizes with single or multiple neuromodulator factors on n-behavior modified Go-NoGo tasks, stop criteria were adjusted to account for the increased behaviors: 1) average trial least square error over last n*25 trials was under threshold of 1, or 2) 15,000 training trials was reached. Performance on the tasks was assessed as before. For overlapping subpopulations, overlap was quantified in two ways. For each network, the number of neurons neuromodulated in 2 or more subpopulations was measured (Extended Data Fig. 6d). Overlap was also quantified by measuring the average number of neuromodulated subpopulations a neuron in the network was a member of (Extended Data Fig. 6e).

Single neuron inputs, functional clustering, and selectivity index. Neural activity in a RNN is a complex function of all the neuron activities tracing all the way back in time. To understand how neuromodulation shifted synaptic inputs at the single neuron level, we considered the first time point in a trial. For any trial, at t=0 all activities are randomly initialized from a normal distribution. As a result, at t=1, a neuron reacts only to the weighted inputs of its incoming connections, uncontaminated by propagating recurrent activity dynamics from past timepoints. Analysis of neuron activity at this timepoint is shown in Extended Data Fig. 7a–c.

In order to examine whether trained models contained functionally specialized neurons, we grouped neuron activities by combination of subtask (which maps one-to-one with neuromodulatory state) and stimulus given ("stimulus-subtask combinations"). We averaged activity of each neuron over time and trials within each group. This resulted in a matrix of time-trial averaged neuron activities with a number of rows equal to the stimulus-subtask combinations, and number of columns equal to the number of neurons. Using k-means, we clustered neurons with similar activity levels across stimulus-subtask combinations. We computed a silhouette score to find the optimal number of clusters, which for the RNN in Extended Data Fig. 7, was 6. The silhouette score computed for 5 and 6 clusters differed only by 0.7% and the additional cluster was very small and similar to an existing cluster, so we conducted further analysis with 5 clusters for simplicity.

To measure the selectivity of individual neurons for particular stimulus-subtask combinations, we

calculated a "selectivity index" (si) for each neuron j:

$$\mathrm{si}_j = \frac{\bar{r}_j^{max} - \bar{r}_j^{second\_max}}{\bar{r}_j^{max}}$$

where $\bar{r}_j$ is the average firing rate of neuron j over the trial duration, $\bar{r}_j^{max}$ indicates the maximum $\bar{r}_j$ across all the stimulus-subtask combinations and $\bar{r}_j^{second\_max}$ indicates the second highest $\bar{r}_j$ over all the stimulus-subtask combinations. The selectivity index thus captures a normalized approximation of how uniquely active a neuron was for a given stimulus-subtask combination.

Network population dynamics. To represent whole network population activity dynamics we sought a low dimensional representation of whole population activity. We used principal component analysis (PCA) since the leading components capture the largest projections of activity variability, which we hypothesized would effectively separate our neuromodulatory conditions if large differences occurred [54]. We found this was the case. We found qualitatively similar results using multidimensional scaling which finds projections designed to best preserve distances in high-dimensional activity space. For our figures we display the first 3 PCs, as these captured a large amount of the activity variance (80–92% explained across the analyses) and effectively represent the activity dynamic differences in the analyses.

To map the neuromodulation-dependent activity subspace, we generated 100 independent stimuli series consisting of random numbers drawn from a uniform distribution between 0 and 1 at each time point (t=0 to t=200) and fed this into the RNN with and without neuromodulation (shotgun stimulus mapping from Extended Data Fig. 10a), which defined non-overlapping subspaces of activity space.

To analyze neuromodulation transition curves we compared activity under intermediate neuromodulation levels with linear interpolation. Linear interpolation was done by evenly dividing the distance between no and full neuromodulation activity states into 9 sections analogous to the 9 neuromodulation levels assessed. These 9 points in activity space were then used to generate output that is plotted in Extended Data Fig. 11. The geometry of the neuromodulation-based transition

was assessed by calculating the Euclidean distance of intermediate neuromodulation level states at a given trial timepoint to the nearest point on the line connecting no and full neuromodulation states at that timepoint. These distances are plotted in Fig 3i. The angle of departure (AoD) was defined as the angle formed by the line between no and full neuromodulation states and the line between no neuromodulation and the first neuromodulation level states, which can be calculated as:

$$\vec{v_1} = \vec{p_F} - \vec{p_N}$$

$$\vec{u_1} = \vec{p_{L1}} - \vec{p_N}$$

$$AoD = cos^{-1} \frac{\vec{u_1} \cdot \vec{v_1}}{|\vec{u_1}||\vec{v_1}|}$$

where $\vec{p_N}$ is the network state with no neuromodulation, $\vec{p_F}$ is the network state with full neuromodulation, $\vec{p_{L1}}$ is the network state with the first level of neuromodulation.

EC50. The EC50 of a network was defined as the level of neuromodulation that led to half the output of full neuromodulation. For the results reported, we used EC50 calculated for the positive stimulus. For this stimulus in the modified Go-NoGo task, a non-neuromodulated network outputs +1 and a fully neuromodulated network outputs 0 (measurements for output level were taken at 0.5 s through the trial); the EC50 for the network in this case is the amount of neuromodulator required to output 0.5. The EC50 was calculated by fitting a sigmoid curve to the progression of output (from +1 to 0 in this case) with increasing neuromodulation level (Fig. 3d)

$$output = 1 - \frac{1}{1 + e^{a \cdot f_{nm} + b}}$$

where f_{nm} is the neuromodulation level. EC50 neuromodulation level was calculated by finding the intersection of the sigmoid and the half-maximal output; for half-maximal output of 0.5, EC50 $= -b/a$. Sigmoid curves were fit using a least squares fit.

***Drosophila* sugar sensitivity task.** We implemented a computational version of Inagaki et al. 2012 to train our network models. During training, models were presented with a constant sugar

concentration (external input proportional to sugar concentration) for 100 timesteps (equivalent to 500 ms) and trained to output a probability of PER. For fed and 2-day starved training we used a piece-wise linear approximation estimated from Inagaki et al. 2012. To compare boxplots of MAT, one-way ANOVA followed by t-test with Bonferroni correction was used as in Inagaki et al. 2012.

MAT. Analogous to the analysis done for flies in Inagaki et al. 2012, for each RNN a sigmoid was fit

$$PER = \frac{1}{1 + e^{-a \cdot log_2 \frac{x_{sugar}}{MAT}}}$$

where a is the slope of the sigmoid. When $PER = 0.5$ then $x_{sugar} = MAT$. Sigmoid curves were fit using a least squares fit.

For intermediate neuromodulatory level (f_{nm}=3) MAT variability analysis, a normalized change in MAT (%ΔMAT) was calculated:

$$\%\Delta MAT = \frac{MAT_{f_{nm}=3} - MAT_{f_{nm}=1}}{MAT_{f_{nm}=5} - MAT_{f_{nm}=1}}$$

where $MAT_{f_{nm}=x}$ is the RNN's MAT with neuromodulation factor x. %ΔMAT gives a network normalized metric for how much the intermediate neuromodulation (f_{nm}=3) moved the fly from no neuromodulation (f_{nm}=1) to full neuromodulation (f_{nm}=5) sensitivity.

Electrical modulation. We administered electrical modulation as an external current applied for the duration of the trial. "On-target" modulation was applied to the neuromodulated neuron population and "random" modulation was applied to a randomly selected group of neurons of equal size; these could include both neuromodulated or non-neuromodulated neurons. All neurons (both excitatory and inhibitory) within the selected subpopulation were given identical external current modulation. For fixed electrical modulation simulations, a current of magnitude 1 was applied (+1 for excitatory modulation; -1 for inhibitory).

For graded electrical modulation, networks that did not achieve e-mod50 at maximum stimulation

(-9 units) were assigned a surrogate e-mod50 value of -10 to calculate correlation to EC50. To account for possible missed correlation due to this substitution, correlation of EC50 to output at maximum modulation (-9) was also calculated (Extended Data Fig. 13c).

Data and code availability

The code and RNN models in this work will be made available at `https://github.com/tsudacode/neuromodRNN`

Extended Data

Extended Data Figures

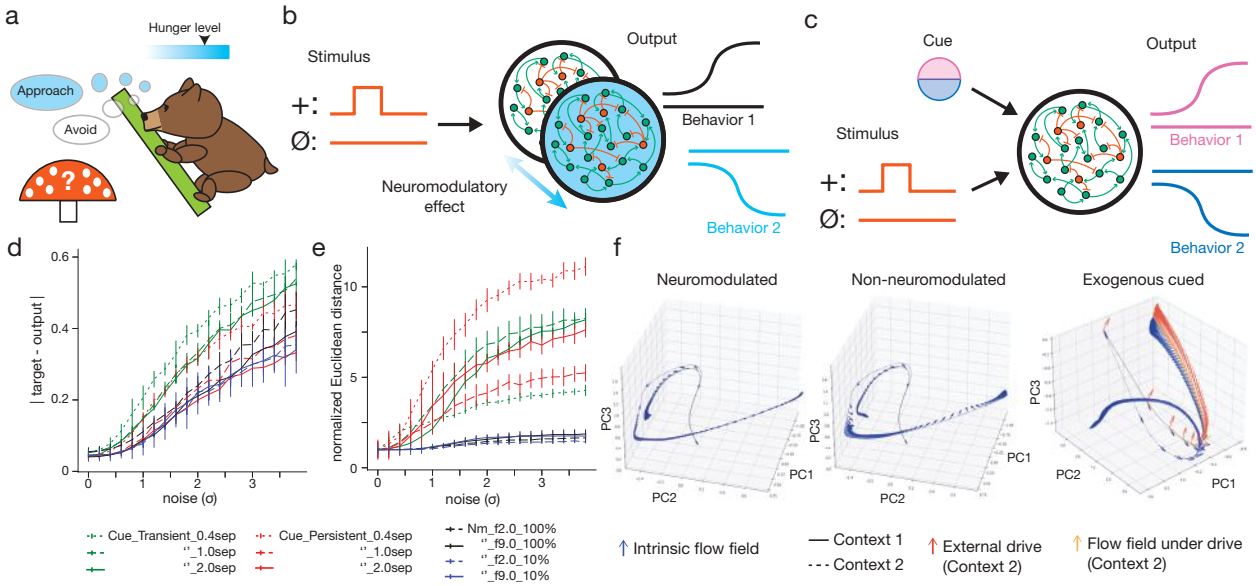

Extended Data Fig. 1 | Noise robustness of neuromodulated and external cue-driven networks. **a**, Neuromodulation is a fundamental biological mechanism, underlying e.g. how hunger level dictates a bear's behavior when encountering a mystery mushroom. **b**, Modified Go-NoGo task in neuromodulated network. Neuromodulatory effect alters network configuration to produce different behaviors. **c**, Standard, context-dependent model with contextual cue input. External cue is required to drive activity to generate different outputs. **d**, Output error for neuromodulated and exogenously cued models with increasing input noise. Noise is drawn from normal distribution with standard deviation σ. Transiently cued models (green) — biologically more realistic than persistently cued (red) — have errors that increase more rapidly with increasing noise compared to neuromodulated (black—100% of network, blue—10% network; dashed lines factor 2.0, solid lines factor 9.0) or persistently cued models (red). **e**, Average Euclidean distance of neural trajectory endpoint between replicates when given no driving input across increasing levels of input noise. Neuromodulated networks (blue, black) generate network dynamics robust to noise, unlike cued models (green, red) which rapidly become unpredictable, exhibiting high variability — measured as increased Euclidean distance of trajectory endpoints on replicate trials — as noise levels increase. Cued models in **d**,**e** are highly dependent on specific cue values and separation amplitude between cues (dotted lines represent networks that had input cue amplitudes separated by 0.4 arbitrary units (au), dashed lines for cues separated by 1.0 au, solid line for cues separated by 2.0 au). **f**, Neuromodulation changes the flow field of the network in activity space (differences of vector fields in left and middle PCA activity plots). Blue vectors represent network's internal flow field (no driving input) along trajectories. Cue-based model (right) relies on external input (red arrows) to drive the network along desired trajectory in phase space (yellow arrows for Context 2 trajectory). For visualization clarity, flow field vectors indicate direction of activity change (without magnitude) and are shown only when network activity is changing more than a threshold of 0.02 units of Euclidean distance per timestep in full network activity space.

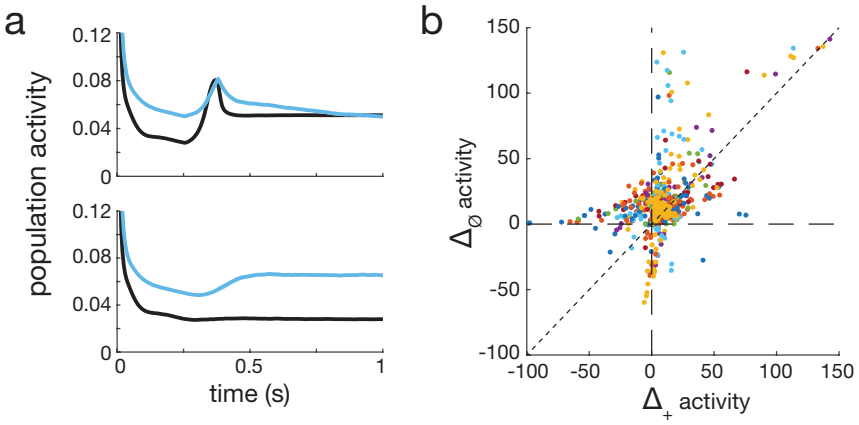

Extended Data Fig. 2 | Neural activity under neuromodulation. a, Mean whole network population activity for example RNN over 100 trials after training. Activity under neuromodulation (blue) is not simple transform of activity without neuromodulation (black). **b**, Difference of mean activity with and without neuromodulation (Δactivity) on + vs $\emptyset$ stimulus trials for individual neurons. Each color represents an independently trained RNN (10 colors total). Points representing simple scaling of neural activity under neuromodulation would lie on dotted diagonal line.

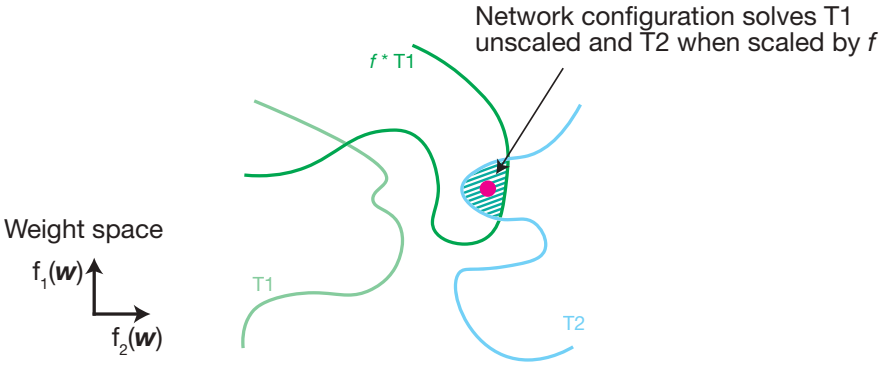

Extended Data Fig. 3 | Relationship between neuromodulated weight configurations. For the contradictory end behaviors in response to shared stimuli, as in the modified Go-NoGo task, a single network without neuromodulation cannot simultaneously learn both tasks as depicted in this schematic by the lack of overlap between weight space that solves task 1 (T1) and task 2 (T2). By scaling weights in the network by a factor f, neuromodulation allows overlap between the f·T1 and T2 spaces. The network solves task 1 when weights are unscaled (T1), and task 2 when weights are scaled (f·T1 ∩ T2).

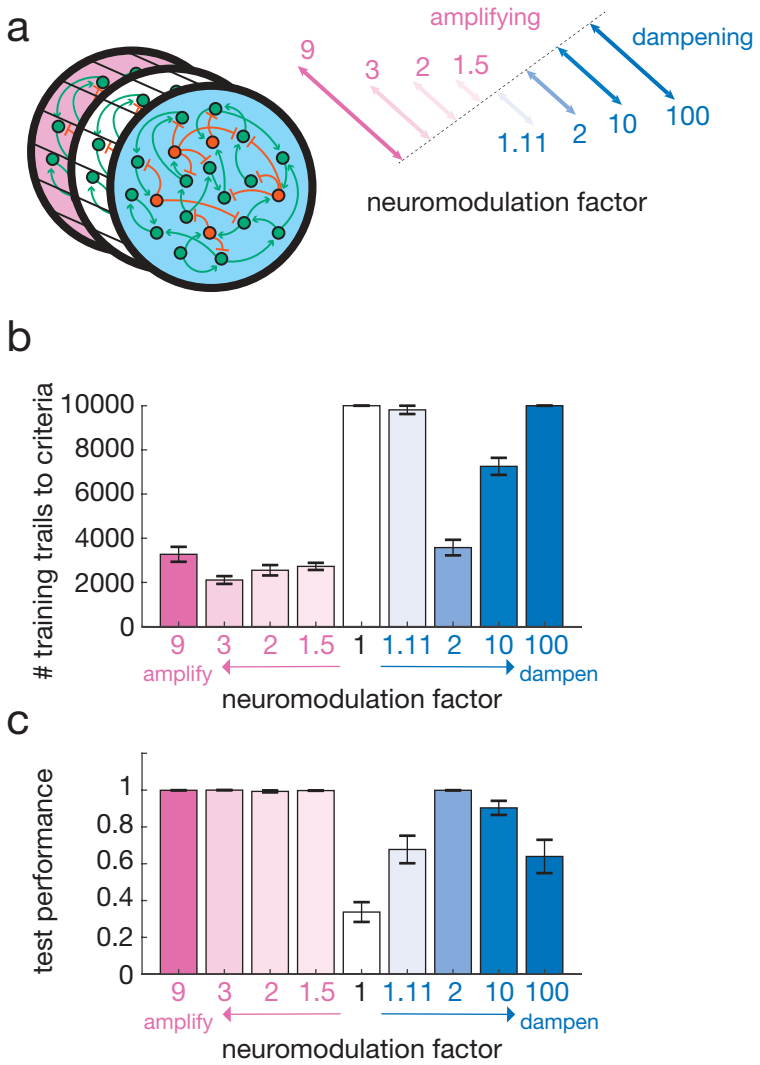

Extended Data Fig. 4 | Neuromodulation weight scaling mechanism works over a range of factors. **a**, A range of neuromodulation factors were tested on the modified Go-NoGo task. Factors were applied to weights initialized as described in Methods. **b**, All amplifying factors tested supported task learning in a similar number of training trials. Dampening factors that were either too small (e.g. 1.11) or too large (e.g. 100) led to longer training. **c**, All amplifying factors tested had perfect task performance. Dampening factors that were either too small or too large led to impaired performance, though better than without neuromodulation (factor=1). Extreme strong dampening effectively silences all transmission between neurons, impairing information flow in the network. Too little scaling (e.g. 1.11 factor dampening) did not create enough separation to distinguish the behaviors.

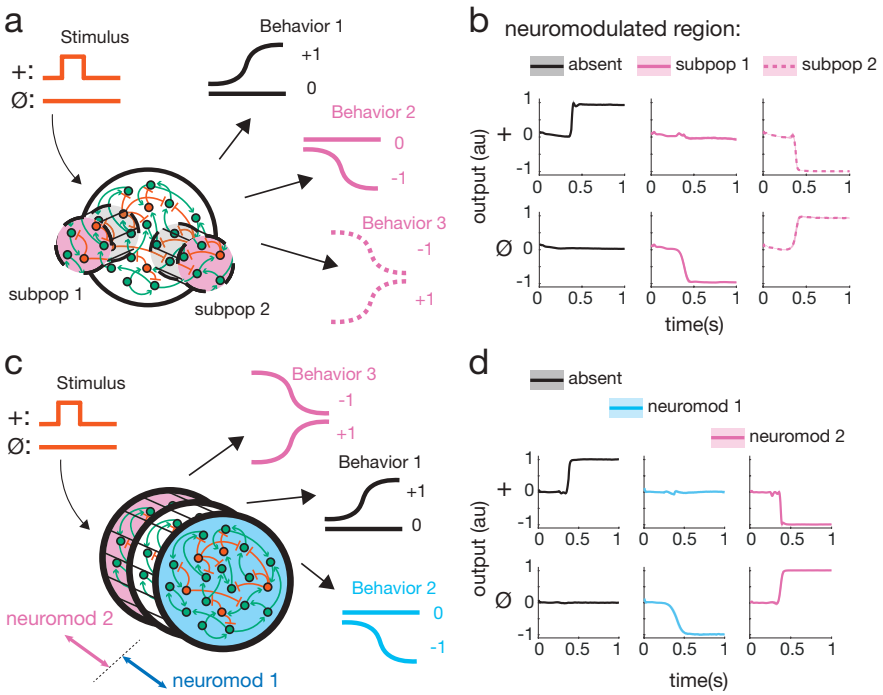

Extended Data Fig. 5 | Multi-neuromodulator RNNs support multiple behaviors. a, 3-behavior modified Go-NoGo. Neuromodulation (factor (f_{nm})=2.5) of either subpopulations ("subpop") within a RNN (subpop1, subpop2) unlock unique behaviors (Behavior 2 (+ stimulus → 0 output, ∅ → -1), Behavior 3 (+ → -1, ∅ → +1), respectively). **b**, Multi-subpop targeted RNN from **a** successfully learns task. Top row: RNN output to + stimulus when different subpops are neuromodulated; bottom row: same for ∅ stimulus. **c**, Same task where different levels of neuromodulation (neuromod 1 (f_{nm}=0.5), neuromod 2 (f_{nm}=1.5)) are applied to whole RNN. **d**, Multi-neuromodulator RNN successfully learns task.

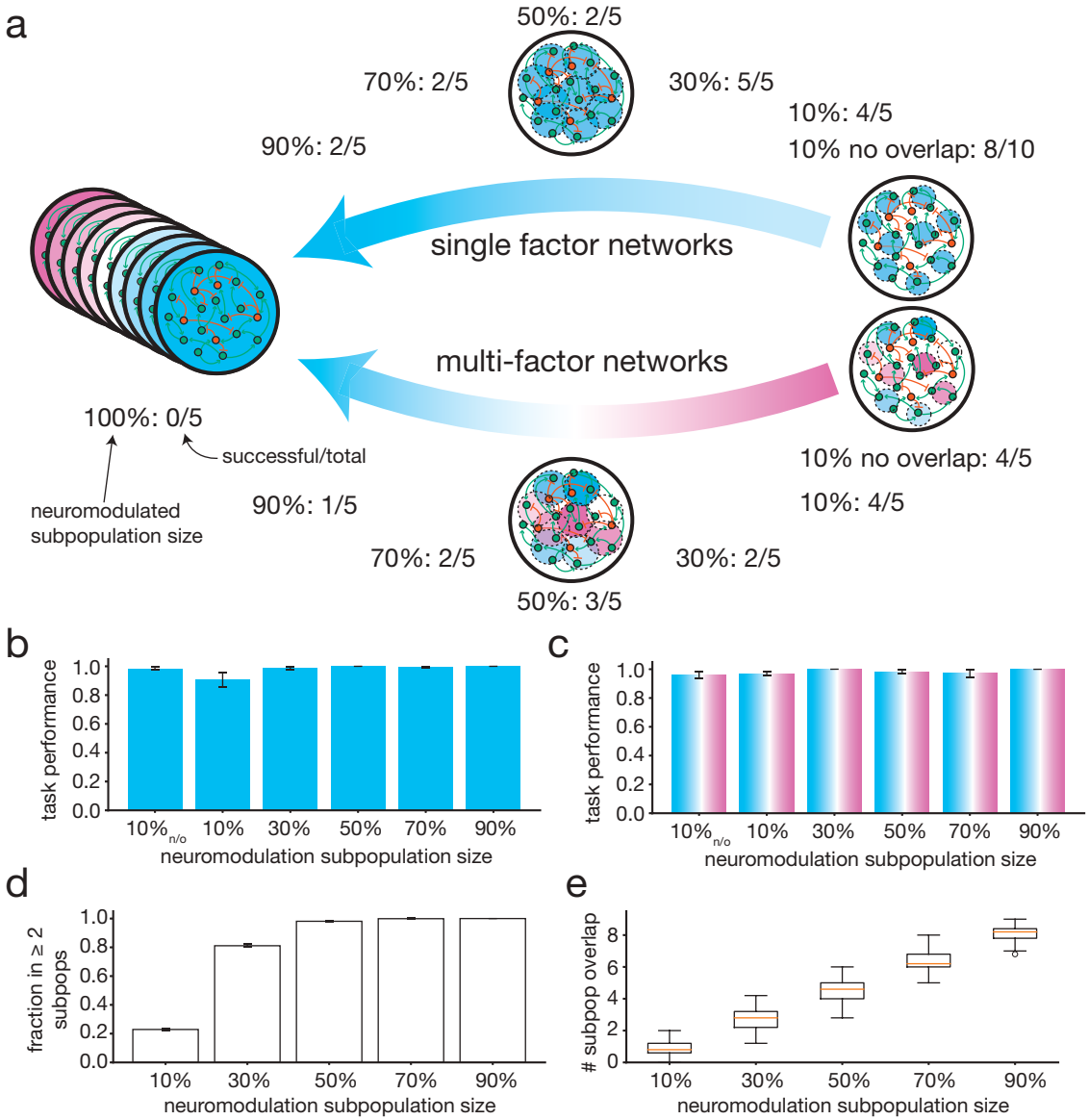

Extended Data Fig. 6 | Spectrum of neuromodulation subpopulation size and factor. a, Different conformations of neuromodulation of a single network support multi-behavior task (9-behavior modified Go-NoGo). Neuromodulation with a single factor (e.g. $f_{nm} = 2.5$) of non-overlapping and overlapping subpopulations across the spectrum of sizes could learn the full 9-behavior task, with larger overlapping subpopulations less consistently learning the full task ("successful/total" refers to independent networks that achieved successful training loss criteria over total attempted). Neuromodulation of the full network with different factors ($f_{nm} \in [1{:}1{:}9]$) consistently supported the 3 behavior task (5/5 successful/total), but not >3 behavior tasks (4-behavior 0/5; 5-behavior 0/5; 9-behavior 0/5 successful/total). Subpopulation neuromodulation with different factors ($f_{nm} \in [1{:}1{:}9]$) could also learn the 9-behavior task with overlapping and non-overlapping subpopulations, similarly exhibiting less consistent learning with larger overlapping subpopulations. **b**, Single factor networks test performance on 9-behavior task across networks that achieved training loss criteria. **c**, Same as **b** but for multi-factor networks. **d**, Fraction of neurons neuromodulated for ≥2 conditions across range of neuromodulated subpopulation sizes. **e**, Mean number of conditions a neuron was neuromodulated for across range of subpopulation sizes. For **d**,**e**, 5 replicates per condition. All error bars are SEM.

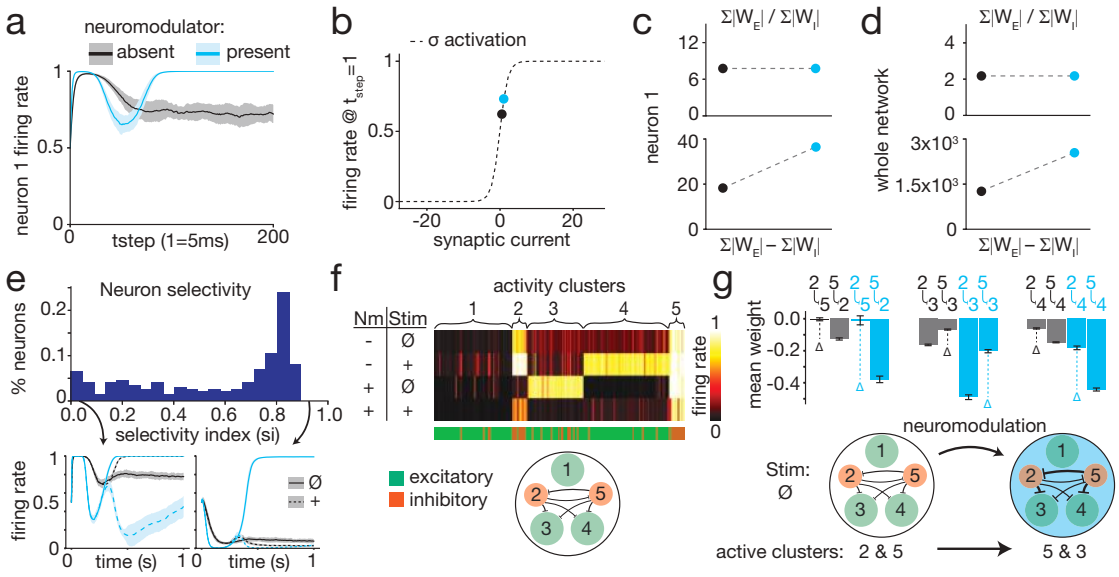

Extended Data Fig. 7 | E-I difference scaling drives differential activity patterns. **a**, Differential response of an individual neuron (neuron 1) in a whole-network neuromodulated RNN to same stimulus depending on neuromodulation presence. **b**, At the start of a trial, neuromodulation causes neuron 1 to receive different synaptic current input, shifting its firing rate. **c**, The different synaptic input under neuromodulation occurs due to amplification of the net difference in incoming excitatory and inhibitory weights; E/I balance is unchanged. **d**, E-I difference across the whole network is also amplified; E/I remains unaltered. **e**, Though all neurons in the RNN are influenced by the same neuromodulation, some exhibited activity selective for particular stimulus-neuromodulation combinations (high si; example neuron bottom right, si=0.89; see Methods); others were less selective (low si; example neuron bottom left, si=0.01). **f**, Neurons formed 5 clusters—2 predominantly inhibitory, 3 predominantly excitatory—whose activity coded for different stimulus-neuromodulation combinations. Each column of the heatmap is the mean firing rate of an individual neuron across conditions with excitatory/inhibitory identity labeled below. (Nm: neuromodulation present or absent; Stim: stimulus presented) **g**, Amplification of relative weight differences (Δs of mean weight) between inhibitory clusters drives cluster activity switches under neuromodulation: increased inhibition of clusters 2 and 4 by cluster 5 and disinhibition of cluster 3. In all panels light blue represents modulator present and grey/white modulator absent. Error bars are SEM.

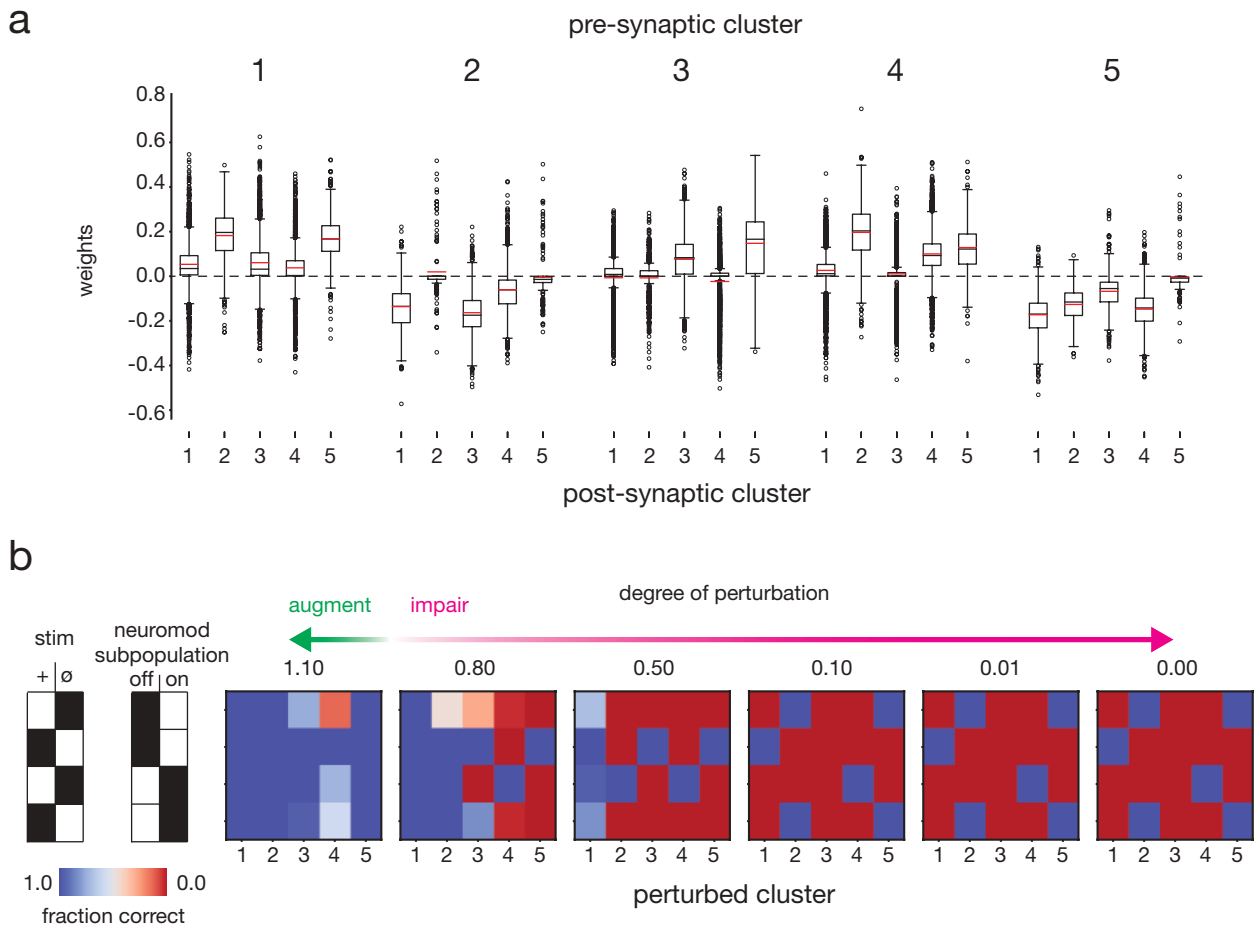

Extended Data Fig. 8 | Inter-cluster weights and functional clustering for network in Extended Data Fig. 7. a, Weight distribution from each cluster (pre-synaptic) to other clusters (post-synaptic). Clusters 2 and 5 were predominantly composed of inhibitory neurons resulting in inhibitory tone on downstream clusters, while clusters 1, 3, and 4 were predominantly excitatory. **b**, Augmentation (perturbation=1.1x) and impairment (i.e., synaptic lesions; perturbation $\in$ [0.80,0.50,0.10,0.01,0.00]x) of specific clusters led to impairment of performance. For most clusters, increased degree of synaptic impairment led to decreased performance, with higher sensitivity for stimulus-context associated clusters (Extended Data Fig. 7f; e.g. cluster 4 for + stim, neuromodulation off). In some stimulus-contexts, strong impairment or full lesion of clusters led to recovery of performance (perturbation ≤ 0.10 for clusters 2 and 5 with null stimulus without neuromodulation or positive stimulus with neuromodulation) suggestive of a counter-intuitive switch in underlying cluster dynamics.

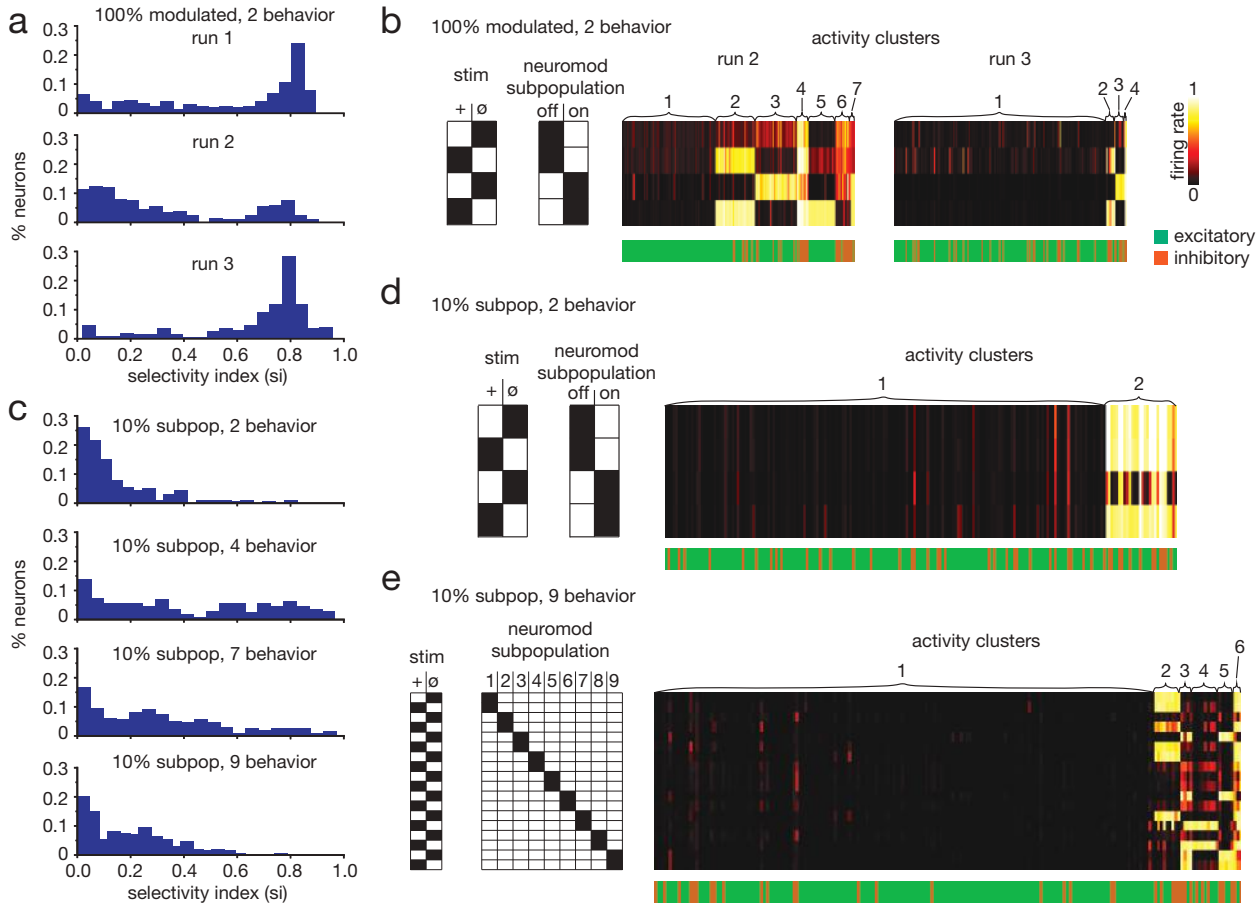

Extended Data Fig. 9 | Independent networks have unique clustering patterns & different network configurations exhibit less selective neurons and complex, overlapping clustering profiles. **a**, Neural selectivity profiles for 3 networks trained independently on the same condition (100% modulated, 2-behavior). All histograms exhibit high selectivity peak. **b**, Each network from **a** exhibits a unique neural activity clustering pattern including number of clusters and excitatory-inhibitory composition of clusters (see Extended Data Fig. 7f for run 1 cluster heatmap). **c**, Selectivity index histograms for example networks with different configurations and tasks. Compared to a network in which all neurons were neuromodulated trained on the 2-behavior modified Go-NoGo, network configurations with smaller neuromodulated subpopulations and more behaviors exhibited less selective neurons and more non-selective neurons. **d**, A network with 10% neuromodulated subpopulation trained on the 2-behavior modified Go-NoGo formed 2 activity clusters, showing high overlap across stimulus-context conditions. **e**, The stimulus-context clustering profile for a network with 10% neuromodulated subpopulations (non-overlapping) trained on the 9-behavior modified Go-NoGo task. Cluster profiles are complex and highly overlapping. **d**,**e** cluster heatmaps and neuron type labels are same as **b**.

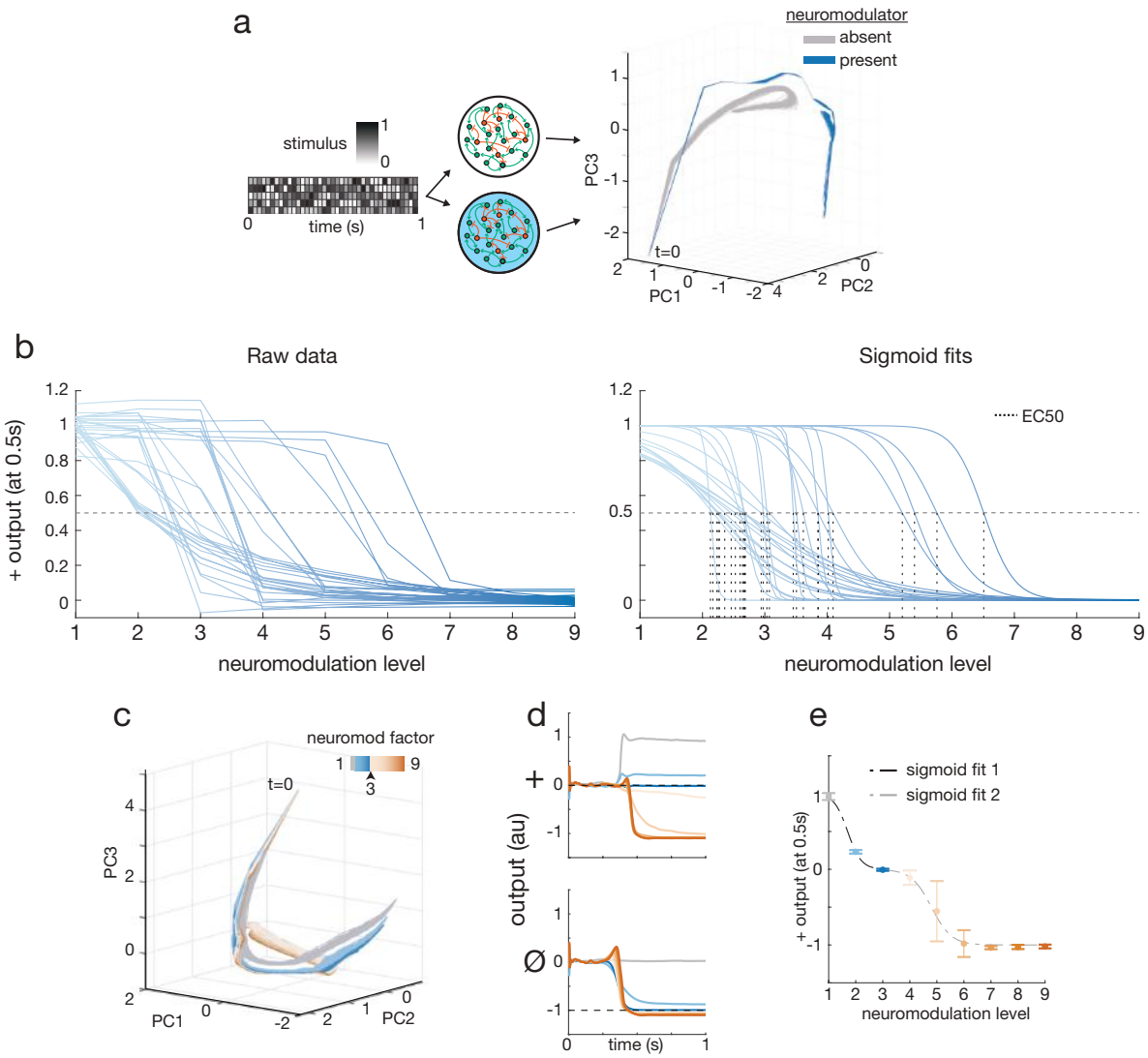

Extended Data Fig. 10 | Variability in network neuromodulatory transitions. **a**, Shotgun stimulus mapping of activity space inhabited by network in absence and presence of neuromodulation defines separable activity manifolds on which individual trajectories occur. **b**, Left: Output to positive stimulus at time point 0.5s of 29 networks at varying levels of neuromodulation. Each network was independently trained with amplifying neuromodulation factor 9 on the modified Go-NoGo task and then tested at intermediate neuromdulation levels. Right: Sigmoid fits to raw data with EC50 of each curve indicated by dotted vertical line. EC50s ranged from 2.1 to 6.5. Slope of sigmoids (σ_slope) ranged from 0.9 to 26.3. **c**, For + stimulus, excessive neuromodulation pushes network activity into different space. **d**, Over-neuromodulation can drive inappropriate behavior (top) or no change (bottom). **e**, Transition dynamics for overmodulation is best fit by double sigmoid; first fits normal neuromodulation transition (blue) and second fits abberant neuromodulation transition (orange). For all PCA, top 3 PCs accounted for 80–92% of activity variance.

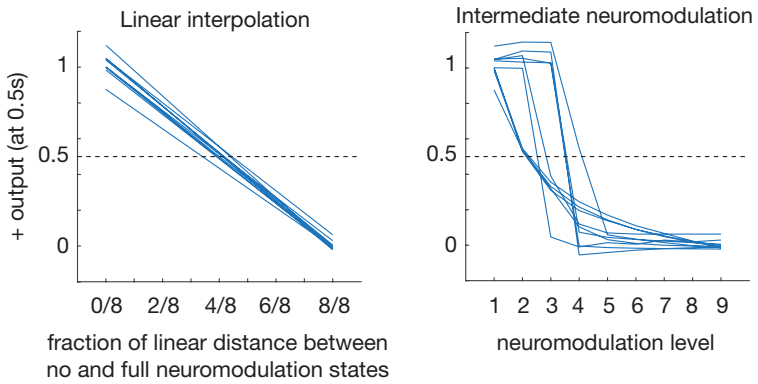

Extended Data Fig. 11 | Unique geometry of transition manifold in phase space leads to highly variable network sensitivity (EC50). Comparison of outputs for pure linear interpolation between no and full neuromodulation states (left) and intermediate neuromodulation levels (right) for same networks. Linear interpolation (left) gives linear output transition, with all networks tightly following a similar transition and intersecting half-maximal output (0.5) very close to the linear interpolation halfway point (4/8 distance). Intermediate neuromodulation (right) results in nonlinear output transition dynamic with high variability. For clarity, plots show only first 10 simulated networks (out of 29 total).

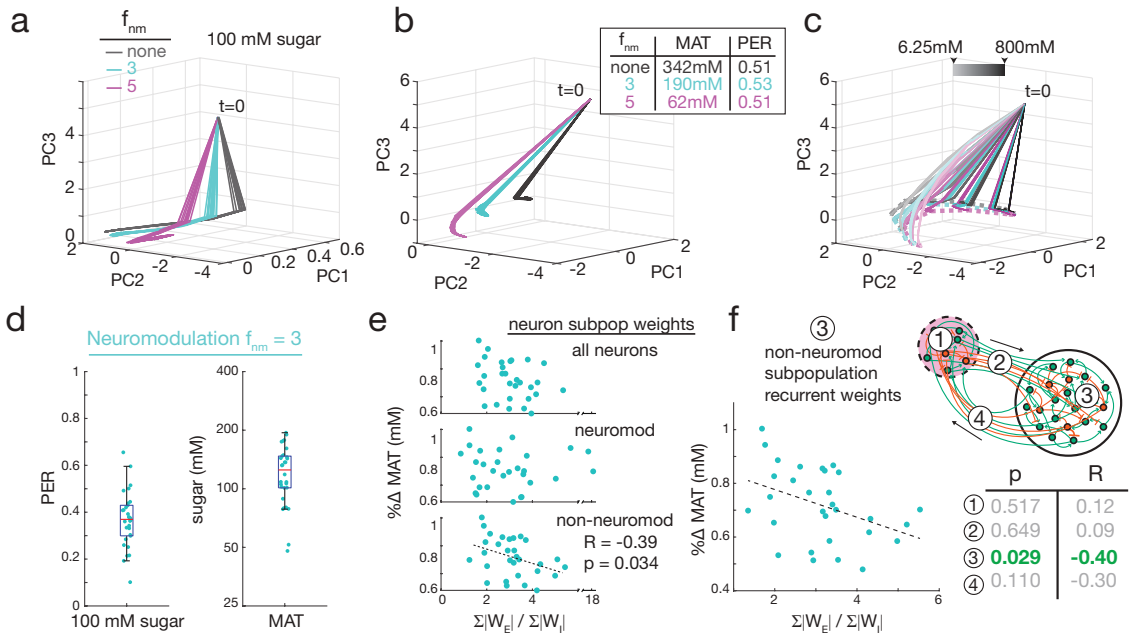

Extended Data Fig. 12 | RNN models of *Drosophila* exhibit emergent transition behaviors and high variability of neuromodulator sensitivity. **a**, For 100mM sugar, a RNN with intermediate neuromodulation (f_{nm}=3; cyan) generates activity between the neuromodulation extremes (none; grey and f_{nm}=5; magenta). **b**, Activity trajectory at MAT sugar concentration for intermediate neuromodulation of a RNN lies between those for neuromodulation extremes. **c**, Across sugar concentrations, intermediate neuromodulation trajectories (cyan) lay between neuromodulation extremes (grey and magenta), forming a 3-layer activity curtain ending on curved line (dotted lines) defined by trajectory endpoints across the sugar spectrum. **d**, Independently trained RNNs (n=30) exhibited high variability of PERs at 100mM sugar (0.10 to 0.66) and MATs (48 to 194mM). **e**, Normalized MAT change (%ΔMAT) vs E/I ratio for whole RNN and subpopulations. %ΔMAT had significant negative correlation to E/I ratio of the non-neuromodulated neurons ($p<0.05$, R=-0.39). **f**, %ΔMAT E/I ratio correlation was driven by recurrent weights within the non-neuromodulated subpopulation ③, rather than recurrent weights within the neuromodulated subpopulation ①, weights from neuromodulated to non-neuromodulated subpopulation ②, or weights from non-neuromodulated to neuromodulated subpopulation ④ as shown by Pearson correlation p-values (p) and coefficients (R) (for ①,②,④ correlation significance scores shown, scatter plots not shown).

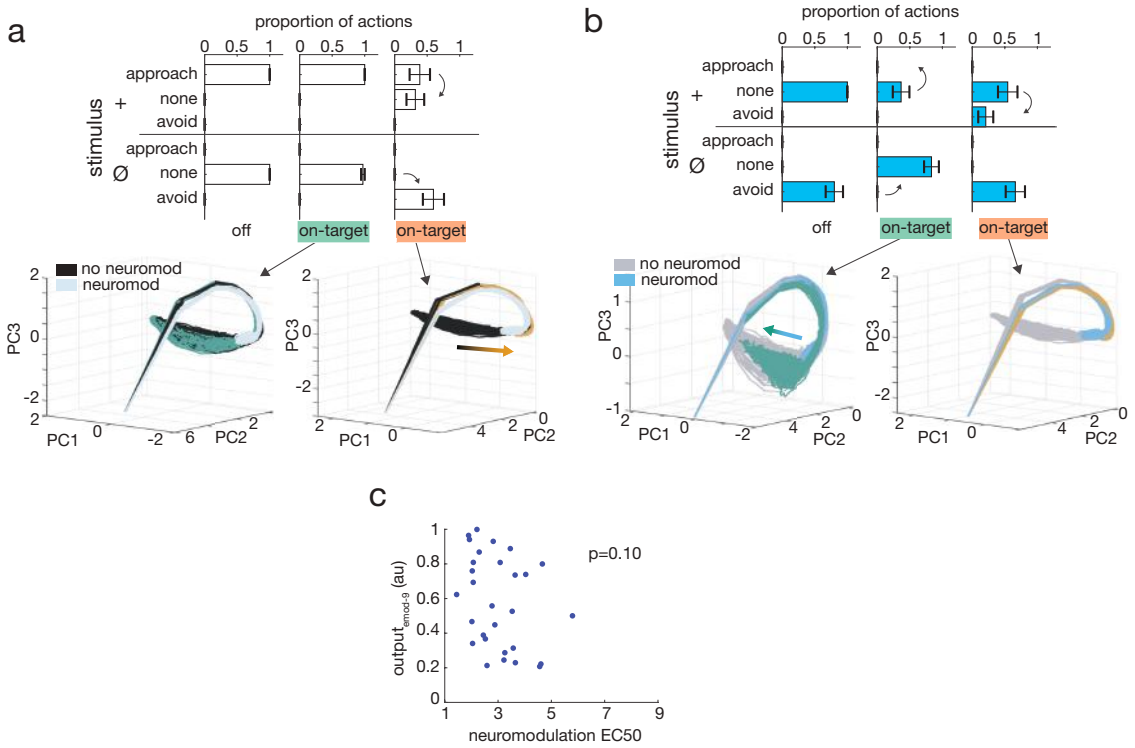

Extended Data Fig. 13 | Targeted electrical modulation shifts network dynamics through independent circuit effect. a, Behavioral and activity shifts in absence of neuromodulation. Top: behavioral shifts with on-target e-mod. Bottom: activity dynamics under e-mod. Activity trajectories without e-mod are in black (neuromodulated trajectories in light blue for reference); e-mod can shift trajectories off black toward neuromodulated activity space (orange arrow). **b**, Same as **a** with present neuromodulation. Top: behavioral shifts. Bottom: Activity trajectories without e-mod are in blue (non-neuromodulated trajectories in grey for reference); e-mod can shift trajectories off blue toward non-neuromodulated activity space (green arrow). **c**, Some networks did not reach an output level equivalent to half the response of maximal neuromodulation (EC50) even at the highest level of electrical modulation given of -9 units. To assess all networks electrical modulation sensitivity in comparison to neuromodulation sensitivity, network output at maximum electrical modulation is compared to EC50. Like EC50 vs e-mod$_{50}$, there is no significant correlation (p=0.10).

Extended Data Appendix

A. Relationship to isolated gain modulation

Gain modulation changes the slope of the unit activation function (the neuron's "intrinsic excitability") by changing a gain parameter g:

$$r = f(x; g)$$

where r is the firing rate and x is the synaptic current variable. For the sigmoid activation function this corresponds to:

$$r = \frac{1}{1 + e^{-gx}}$$

To see the effective change on the activation function of amplifying or dampening the weights we can compare the effect of gain modulation to weight modulation on the equation that governs neural dynamics:

$$\tau \dot{x}_i = -x_i + \sum_j W_{ji} r_{ji} + W_{ui} u + N(0, 0.1)$$

If we assume no input and no noise, we get a simplified equation describing neuron dynamics:

$$\tau \dot{x}_i = -x_i + \sum_j W_{ji} r_{ji}$$

Gain modulation g gives:

$$\tau \dot{x}_i = -x_i + \sum_j W_{ji} r_{ji}(g)$$

while weight modulation with a neuromodulation factor m gives

$$\tau \dot{x}_i = -x_i + \sum_j m \cdot W_{ji} r_{ji}(1)$$

To compare each type of modulation, we can consider the modified terms:

$$1 \cdot r(g) = \frac{1}{1 + e^{-gx}} \qquad \text{(gain effect)}$$

$$m \cdot r(1) = \frac{1}{\frac{1}{m} + \frac{1}{m} \cdot e^{-x}} \qquad \text{(weight effect)}$$

$$= \frac{1}{\frac{1}{m} + e^{-x - ln\, m}}$$

These effects are equivalent when

$$g = -\frac{ln(\frac{1-m}{m} + e^{-x - ln\, m})}{x} \tag{1}$$

So generally gain modulation, g, is only equivalent to a weight modulation by m if the gain term is precisely the time varying function of x defined by equation (1). Furthermore, for some values of m, there is no equivalent g for certain values of x. E.g. for $m = 2$, g is defined by equation (1) only for $x < 0$. For arbitrary values of x with fixed, constant g and m:

$$r_{ji}(g) \neq m \cdot r_{ji}(1)$$

except when $g = m = 1$, i.e., when there is no modulation. Thus, weight neuromodulation and gain modulation operate through different effects.

B. Chemical and electrical modulation

Chemical (neuromodulation) and electrical modulation in our network operate in directionally similar manner with qualitatively different effects. This can be seen by inspecting the equation governing each neuron i's synaptic current variable and thereby the network's activity dynamics:

$$\tau \dot{x}_i = -x_i + \sum_j W_{ji} r_{ji} + W_{ui} u + N(0, 0.1)$$

For any given neuron we can break up the terms by whether an input neuron is in the neuromodulated subpopulation or not:

$$\tau \dot{x}_i = -x_i + \sum_k W_{ki} r_{ki} + \sum_q W_{qi} r_{qi} + W_{ui} u + N(0, 0.1)$$

where k is the index for non-neuromodulated neurons and q is the index for neuromodulated neurons.

Neuromodulation in our model acts by scaling the target neurons outgoing weights by a factor f:

$$\tau \dot{x}_i = -x_i + \sum_k W_{ki} r_{ki} + f \cdot \sum_q W_{qi} r_{qi} + W_{ui} u + N(0, 0.1)$$

Electrical stimulation acts by adding exogenous synaptic current to target neurons. For a given neuron i in the non-neuromodulated subpopulation, electrical stimulation of the neuromodulated subpopulation is felt through altered incoming firing rates:

$$\tau \dot{x}_i = -x_i + \sum_k W_{ki} r_{ki} + \sum_q W_{qi} r_{qi,Estim} + W_{ui} u + N(0, 0.1)$$

and a neuron i in the neuromodulated subpopulation is additionally affected through direct stimulation:

$$\tau \dot{x}_i = -x_i + \sum_k W_{ki} r_{ki} + \sum_q W_{qi} r_{qi,Estim} + W_{ui} u + u_{Estim} + N(0, 0.1)$$

Thus we can see that both chemical and electrical stimulation act through the same term in the equation that governs neural synaptic currents yet in different manners. Neuromodulation directly scales presynaptic weighted inputs from neuromoduated neurons, whereas electrical stimulation acts by altering the firing rate of presynaptic neuromoduated neurons with an additional direct influence on the synaptic current if the neuron of interest is in the electrically stimulation subpopulation.

The similarities of these forms of modulation (acting through the same terms of the synaptic current equation) indicates why they can have similar affects on network output in some circumstances. Nevertheless, the differences in how they affect the synaptic current equation are propagated through the recurrent connections of the network at each time step which drives the distinct dynamical changes seen under chemical versus electrical modulation.